Graphical Abstract

AquaFeL-PSO: An Informative Path Planning for Water Resources Monitoring using Autonomous Surface Vehicles based on Multi-modal PSO and Federated Learning

Micaela Jara Ten Kathen, Federico Peralta, Princy Johnson, Isabel Jurado Flores, Daniel Gutiérrez Reina

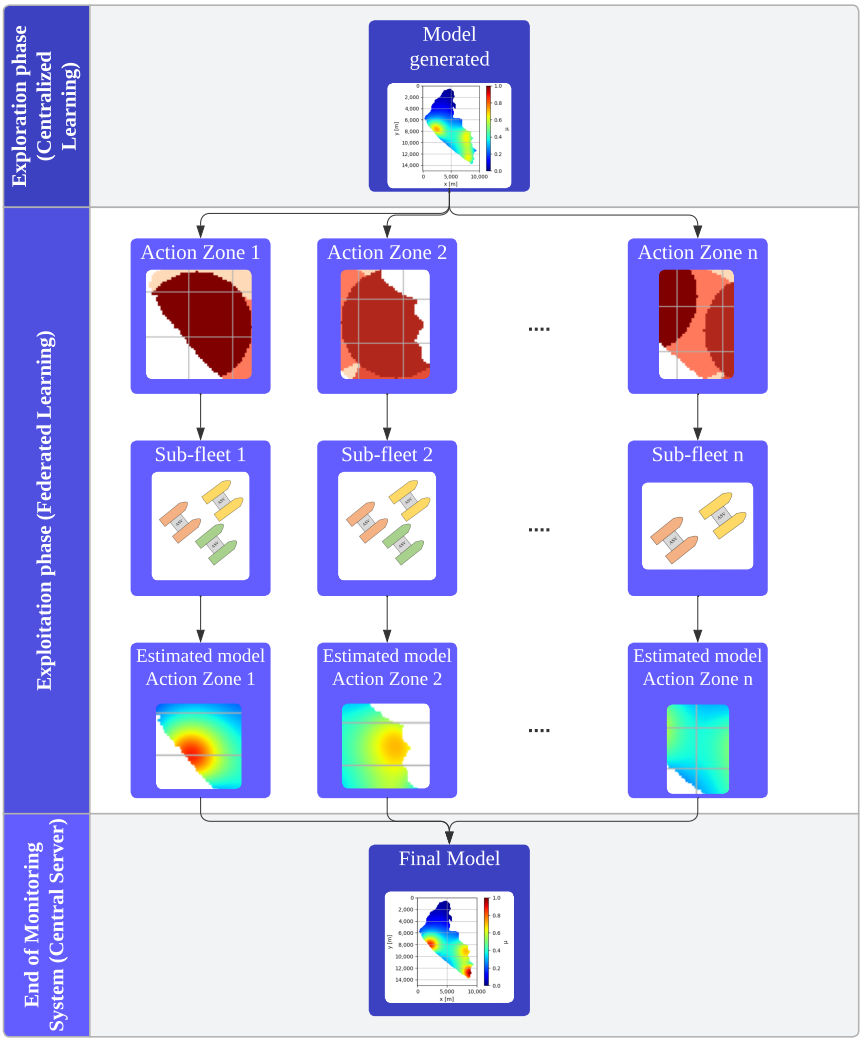

Highlights

AquaFeL-PSO: An Informative Path Planning for Water Resources Monitoring using Autonomous Surface Vehicles based on Multimodal PSO and Federated Learning

Micaela Jara Ten Kathen, Federico Peralta, Princy Johnson, Isabel Jurado Flores, Daniel Gutiérrez Reina

- Informative path planning based on PSO, Gaussian process and federated learning.
- The AquaFeL-PSO excels in various water monitoring tasks.
- The AquaFeL-PSO outperforms other PSO-based algorithms in mean square error.
- Federated learning validated for water estimation models with autonomous vehicles.

AquaFeL-PSO: An Informative Path Planning for Water Resources Monitoring using Autonomous Surface Vehicles based on Multi-modal PSO and Federated Learning

Micaela Jara Ten Kathen[a,b,*], Federico Peralta[c], Princy Johnson[d], Isabel Jurado Flores[c], Daniel Gutiérrez Reina[e]

[a]*Facultad de Ciencias y Tecnología, Universidad Católica "Nuestra Señora de la Asunción", Supercarretera, s/n, Hernandarias, 100519, Alto Paraná, Paraguay*
[b]*Fundación Parque Tecnológico Itaipú, Supercarretera, Hernandarias, 100519, Alto Paraná, Paraguay*
[c]*Department of Engineering, Universidad Loyola Andalucia, Av. de las Universidades, s/n, Dos Hermanas, 41704, Seville, Spain*
[d]*School of Engineering, Liverpool John Moores University, Byrom St., Liverpool, L3 3AF, Merseyside, United Kingdom*
[e]*Department of Electronic Engineering, Technical School of Engineering of Seville, C. Americo Vespucio, Seville, 41092, Seville, Spain*

Abstract

The preservation, monitoring, and control of large water resources has been a major challenge in recent decades. To ensure the quality of water resources, it is necessary to constantly monitor pollution levels. To meet this objective, this paper proposes an informative path planning for water resource monitoring, namely the AquaFeL-PSO algorithm, which uses autonomous surface vehicles, equipped with water quality sensors, based on a multi-modal particle swarm optimization, and the federated learning technique, with Gaussian process as a surrogate model. The proposed informative path planning has two phases, the exploration phase and the exploitation phase. In the exploration phase, the vehicles examine the surface of the water resource, and

*Corresponding author
Email addresses: micaela.jara@uc.edu.py (Micaela Jara Ten Kathen), fdperalta@uloyola.es (Federico Peralta), p.johnson@ljmu.ac.uk (Princy Johnson), ijurado@uloyola.es (Isabel Jurado Flores), dgutierrezreina@us.es (Daniel Gutiérrez Reina)

with the data acquired by the water quality sensors, an initial water quality model is estimated in the central server. In the exploitation phase, the area is divided into action zones using the model estimated in the exploration phase for a better exploitation of the contamination zones. To obtain the final water quality model of the water resource, the models obtained in both phases are combined. The results demonstrate that the proposed AquaFeL-PSO path planner is 3% more efficient in obtaining water quality models of the action zones than other similar path planners compared in this article. Moreover, in this case study, the AquaFeL-PSO has been demonstrated to have 300% more efficiency in achieving a better model of the entire water resource, and approximately 4,000% improvement in detecting pollution peaks. The analysis of variance provides support for these results, demonstrating a significant difference between the means of the path planners in detecting pollution peaks and generating the water quality model of the entire surface of the water resource. It was also shown that the results obtained by applying the federated learning technique are very similar to that of a centralized system and it allows to obtain a model of the water resource even when the Gaussian process of an action zone does not converge.

Keywords: Water resource monitoring, Autonomous surface vehicle, Informative path planning, Particle swarm optimization, Gaussian process, Federated learning

---

Nomenclature

t	Time.
$\mathcal{P}$	Set of vehicles in the fleet.
$p \in \mathcal{P}$	A vehicle.
$\mathcal{S}$	Water quality parameter sensors.
$s \in \mathcal{S}$	A water quality parameter sensor.
$\mathcal{M}$	Set of measures taken by the ASV fleet.
$\mathcal{N} \subset \mathbb{R}^2$	Set of coordinates within a 2D space.
$\mathbf{x} \in \mathcal{N} = (x, y)$	A location, coordinate.
$\mathcal{Q} \subset \mathcal{N}$	Set of coordinates where the fleet measured water quality values.
$\mathcal{U} \subset \mathcal{N}$	Set of all coordinates where any of the ASVs in the fleet where located.
$\mathcal{U}_{(p)} \subseteq \mathcal{U}$	Subset of the coordinates through which the ASV p passed.
$\mathcal{A} \subset \mathcal{N}$	Set of all action zones.
$\mathcal{P}_{(a)} \subseteq \mathcal{P}$	Subset of the vehicles assigned to the action zone a.
$y(\mathbf{x})$	Ground truth value of the water quality parameter at location $\mathbf{x}$.
$\hat{y}(\mathbf{x})$	Estimated model value of the water quality parameter at location $\mathbf{x}$.
K	Covariance (kernel) matrix of the Gaussian Process.
$\mu_s(\mathbf{x})$	Mean value estimated by a Gaussian Process of the water quality parameter s at location $\mathbf{x}$.
$\sigma_s(\mathbf{x})$	Uncertainty value obtained by a Gaussian Process of the water quality parameter s at location $\mathbf{x}$.

1. Introduction

Water is fundamental to life. Although it is a renewable resource, its availability is decreasing worldwide. Freshwater reservoirs are being polluted by domestic and industrial effluents and fertilizers from agricultural activities, among other sources. These problems not only affect the quality of human life, but also the health of the planet. In 2015, during the United Na-

tions Summit, the 2030 Agenda for Sustainable Development was approved[1], which establishes 17 Sustainable Development Goals and 169 targets to improve people's lives, protect the planet and foster prosperity. The sixth goal focuses on ensuring the availability of water and its sustainable management and sanitation for all, promoting the reduction of pollution, the efficient use of water resources and the development of water-related programs [1].

A crucial method for facilitating the progress of measures taken to reduce pollution of water resources is the continuous monitoring of water quality. Water bodies under constant threat of pollution must be monitored on a permanent basis. An example of this type of monitoring is the Ypacarai lake in Paraguay, where pollution is constantly studied and monitored [2][3]. The main cause of contamination is the domestic and industrial effluents that flow into the lake and its watersheds [4]. As a result, levels of fecal coliforms and nutrients such as phosphorus and nitrate are elevated, leading to the proliferation of cyanobacteria [5]. This problem affects public health, the economy of the region, and the ecosystem of the lake and its surroundings.

The traditional method of water quality monitoring consists of taking samples at specific points in the water resource and analyzing them in specialized laboratories. This method can be exhausting, time consuming, can be subject to human error, and has high costs associated with hiring personnel and equipment [6]. New technologies are currently being investigated, such as aquatic submarines, surface vehicles and aerial drones equipped with sensors capable of measuring water parameters [7][8][6][9]. These vehicles are equipped with Guidance, Navigation and Control (GNC) systems that allow them to move autonomously through the water body. In our previous work, one of the vehicles of the Autonomous Surface Vehicles (ASVs) fleet, Fig. 1, was used to perform control and navigation tests in the Lago de la Vida (Dos Hermanas, Spain)[2] and in the lake of the Alamillo Park (Seville, Spain).

[1] https://sdgs.un.org/es/goals

[2] `https://www.youtube.com/watch?v=3nYzSSGeyHw`

Figure 1: An Autonomous Surface Vehicle used for water resources monitoring.

This work focuses on the guidance system for the ASV fleet. This system generates the path and speed to be followed by the autonomous vehicles. A widely studied algorithm used as basis for the proposed informative path planner is the Particle Swarm Optimization (PSO) [10][11][12], which is easy to implement and requires few parameter settings, although it faces challenges such as initial setup and tendency to stay at local optima [13]. Water resources monitoring is a multi-modal problem due to the presence of multiple pollution zones. Therefore, a multi-modal PSO-based informative path planner is developed using a Gaussian Process (GP) as the underlying model. The monitoring is divided into two phases: exploration and exploitation. In the exploration phase, ASVs cover as much area as possible to obtain an initial model of the water resource, applying centralized learning techniques. Then, in the exploitation phase, high contamination zones are identified and assigned to obtain a more detailed water quality model, using Federated Learning (FL) techniques. This approach allows a precise characterization of pollution zones.

The main contributions of this work are:

- The development of an informative path planning for water resource monitoring based on multi-modal particle swarm optimization and Gaussian process for autonomous surface vehicles that is capable of generating accurate and precise estimated water quality models, and is able to detect areas of water resource contamination in real-time through those autonomous vehicles.

- The application of the informative path planning for the case of the Ypacarai lake, demonstrating in simulation the efficiency and effectiveness of the proposed approach over other path planners.
- The comparison of centralized and federated learning for multi-modal estimation of water quality parameters in water bodies.

The paper layout is as follows: in Section 2, the state of the art of path planners for ASVs and PSO-based algorithms for multi-modal problem solving is presented. The monitoring problem as well as the assumptions made to carry out the monitoring tasks are explained in Section 3. Section 4 summarises relevant path planner algorithms in this application space that are compared with the proposed approach. The proposed informative path planning is presented in Section 5. Section 6 presents the simulation setup, evaluation of the proposed approach, and comparison of the performances of the path planners. Section 7 provides a discussion of the results. Conclusions of the work and future research directions are presented in Section 8.

2. Related work

Water resource monitoring has been studied extensively, and several techniques have been proposed for using ASV in this context. These techniques include Genetic Algorithms (GA), Deep Reinforcement Learning (DRL), Bayesian Optimization (BO), and others, each providing unique solutions to the challenges of water resource monitoring. The first subsection of the related work reviews these methodologies in detail. The second subsection focuses on advances in PSO, highlighting improvements made to address the limitations of multi-modal problems.

2.1. Water monitoring system based on ASVs

In recent years, numerous studies have focused on the monitoring and patrolling of water resources using ASVs)[5][6][14]. To effectively monitor water bodies, these vehicles are equipped with sensors capable of measuring various water quality parameters such as ammonium, pH, and temperature. Additionally, they are often fitted with a Global Positioning System (GPS), an Inertial Measurement Unit (IMU), and/or a camera to enhance their monitoring capabilities.

For the development of ASV guidance systems for monitoring and patrolling tasks, various artificial intelligence techniques have been explored, including GA [5], Swarm Intelligence (SI) [13], BO [8], and DRL [15].

GA, which are meta-heuristic algorithms inspired by the theory of natural selection of Charles Darwin [16][17][18], have been effectively used as path planners. For example, the authors of [19] modeled the monitoring problem as a Traveling Salesman Problem (TSP) where an ASV must cover the largest possible area of a water resource, using fixed beacons on the shore. This work was later extended in [20], where the problem was redefined as the Chinese Postman Problem (CPP), allowing the vehicle to pass through beacons multiple times, thereby maximizing lake surface exploration. A two-phase GA-based monitoring system was further developed in [5], with the first phase focused on detecting contamination areas and the second phase on exploiting the data from these zones.

DRL has also been employed to address water resource monitoring. In [15], the problem was modeled as a Markov Decision Problem, and an online global path planner was developed for ASVs to patrol the Ypacarai lake using RGB images to represent vehicle positions and states. A tailored Deep Q-learning method based on convolutional neural networks was trained using a specific reward function. This work was expanded in [6], where a centralized multi-agent monitoring system was developed, showing that a centralized approach outperforms distributed Q-learning for directed patrolling problems. A comparison between GAs and DRL for ASV monitoring was conducted in [21], demonstrating that DRL excels in complex scenarios while GAs provide robust solutions for low-dimensional scenarios.

Another technique applied is BO. BO has been used in informative path planning, as demonstrated in [8], where the classical BO framework was adapted for water monitoring using GP as a surrogate model. The approach aimed to estimate pollution levels in the Ypacarai lake, comparing different acquisition functions to identify optimal measurement positions. This work was extended to a multi-objective problem in [14], considering multiple water quality parameters and employing various techniques to optimize sampling positions. Further, [22] explored a multi-agent system where multiple ASVs were equipped with sensors for different water quality parameters.

Path planners based on PSO were developed in [13] and [23]. In [13], an informative path planner was created by integrating PSO components with data from an estimated water quality model generated by GP. This algorithm was compared with other PSO-based algorithms in [24] and [25]. The

former focused on exploring the water resource surface to obtain a reliable lake model, while the latter aimed to exploit areas with high pollution peaks. [23] proposed a path planner combining PSO and Grey Wolf Optimization (GWO), demonstrating efficient path generation that expertly avoids obstacles.

2.2. PSO and multi-modal problems

The classical PSO algorithm, while easy to implement and requiring only a few initial parameters, often struggles with getting stuck in local optima and the challenge of setting appropriate initial parameter values [13]. To address these limitations, various strategies have been introduced, including mutation mechanisms, dynamic parameters, and neighborhood techniques.

One method to enhance PSO is incorporating mutation operators to maintain population diversity and prevent premature convergence. For example, in [26], a dynamic inertia weight was combined with a mutation mechanism to balance exploration and exploitation effectively. Similarly, [27] employed Gaussian, Cauchy, and Lévy mutation strategies, selecting the best mutation operator based on the selection ratio. This approach demonstrated that different mutation operators might be more effective depending on the problem type.

Neighborhood information can also improve PSO performance. [28] introduced a dynamic ϵ-neighborhood selection mechanism, adjusting neighborhood size dynamically and employing four position-update strategies based on particle behavior. This approach effectively solved multi-modal problems but struggled with high-dimensional cases. In [29], a dynamic neighborhood-based learning strategy replaced the global learning strategy, with particle velocity updates based on the best positions in their neighborhood. An offspring competition mechanism further enhanced this approach.

Sub-population strategies have also been explored. [30] divided the particle swarm into sub-populations, updating velocities based on the best sub-population positions rather than the entire swarm. This concept was extended in [31], dividing the swarm into groups focusing on global maxima and minima. [32] introduced a cluster-based PSO with a leader updating mechanism and ring topology to improve information exchange between sub-populations.

Our work addresses several gaps in the existing literature. Previous PSO-based path planners focused on GP for model estimation but did not tackle issues of local maxima/minima or multi-modal scenarios [25][13][24]. These

approaches were limited to simple scenarios with a single global maximum, whereas real scenarios often feature multiple contamination peaks. Furthermore, previous studies on multi-agent systems for water monitoring did not apply federated learning [6][14], relying instead on centralized systems. Our research pioneers the application of federated learning for ASV-based water monitoring, reducing communication congestion between vehicles and the main server. Additionally, our approach advances model estimation, achieving low Mean Squared Error (MSE) with techniques that integrate exploration and exploitation phases, surpassing the results of epsilon greedy algorithms and other methods [5].

3. Problem formulation

The primary challenge of the water monitoring task lies in obtaining reliable models of the water quality parameters of the water resource. To address this challenge, the each ASV p in the monitoring system is equipped with sensors $\mathcal{S}$, where S denotes the total number of water quality parameters being monitored. In this study, the monitoring task focuses on a single objective, hence $S = 1$. These sensors measure water quality parameters (m_k). In simulations, a ground truth model of the water resource is employed, represented by the function $y(\mathbf{x})$, where $\mathbf{x}$ denotes the (x, y) coordinates of the water resource. Throughout the monitoring task, M measurements are acquired by the ASV sensors and stored in the set $\mathcal{M}$. Additionally, the coordinates where these measurements are taken are recorded in the set $\mathcal{Q}$.

Applying the regression model, Eq. 1, and having the necessary amount of data, $\mathcal{M}$ and $\mathcal{Q}$, an estimated water quality model $\hat{y}(\mathbf{x})$ of the Ypacarai lake can be obtained.

$$\hat{y}(\mathbf{x}) \approx y(\mathbf{x}) \tag{1}$$

In order to simplify the nomenclature of the data obtained from the measured values of the parameters $\mathcal{M}$ and the coordinates where these measurements were taken $\mathcal{Q}$, consider the set $\mathcal{D}$ as the set containing all the data obtained.

The main objective of this study is to minimize the error between the estimated model generated by the proposed informative path planning $\hat{y}(\mathbf{x})$ and the actual model of water quality parameters in the water resource $y(\mathbf{x})$, constrained by a maximum allowable distance max_dist that the ASVs can travel. This can be observed in Eq. 2:

$$
\begin{aligned}
min \quad & f(\mathbf{x}) = \frac{1}{N}\sum_{i=1}^{N}(y(\mathbf{x}_i) - \hat{y}(\mathbf{x}_i))^2 \\
s.t. \quad & \frac{1}{P}\sum_{p=1}^{P} dist\_ASV_p \leq max\_dist
\end{aligned}
\tag{2}
$$

Here, $f(\mathbf{x})$ represents the MSE between $y(\mathbf{x})$ and $\hat{y}(\mathbf{x})$. The total number of vehicles in the fleet is represented by the term P, while N represents all available coordinates within the search space.

The following assumptions were made for the monitoring system:

Assumption 1. The matrix $\mathcal{R}$ represents the model space of the Ypacarai Lake. The model is structured as an $r \times n$ matrix where each element $\mathcal{R}i, j$ denotes the state of a grid cell. ASVs are permitted to navigate only to grids that have a value of 1. In Fig. 2, available grids are depicted in black. Grids with a value of 0, shown in white, are off-limits to ASVs due to factors such as being land, restricted zones, or obstacles. In simulations, the values of $\mathcal{R}i, j$ are scaled so that each grid measures 100 m x 100 m.

Figure 2: Model of the occupancy grid of the Ypacarai lake.

Assumption 2. The movements of the ASVs are error-free and synchronized. The vehicles are equipped with local path planning that allows them

to deflect obstacles and prevent collisions. The maximum speed at which the ASVs can travel is 2 m/s. Additionally, the starting points of the vehicles are assigned to ports or clear areas around the lake.

Assumption 3. The algorithm incurs the lowest possible cost for the number of measurements taken, signifying minimal sensor operation expenses. The primary factor influencing the monitoring mission is the autonomy of the ASV, with its battery power enabling coverage of up to 30,000 meters.

Assumption 4. There are no communication errors or disconnections in the communication between the vehicle and the central server. In addition, the vehicles communicate only with the central server and not with each other. The initiation of the monitoring task is given by the central server, ensuring that all vehicles start simultaneously.

Assumption 5. The physico-chemical variables measured in this study - pH, temperature, conductivity and turbidity - are assumed to be sufficiently smooth to be modeled effectively using GP. These variables usually exhibit smooth continuous variability, which justifies the use of GPs for their modeling. Measurements of these parameters are taken through sensor probes onboard the ASVs. The measurements are captured in real-time via the onboard sensors and transmitted to the central server. The physical-chemical parameter sensors are in excellent condition and are well calibrated. Therefore, there are no errors in the measurement of water quality parameters.

4. PSO-based path planners

This section describes different versions of PSO-based path planners for water monitoring with ASV.

4.1. Classic Particle Swarm Optimization (PSO)

The PSO algorithm, introduced by Kennedy and Eberhart [33], is an optimization technique inspired by the collective behavior of organisms like fish schools and bird flocks. In PSO, potential solutions to the optimization problem are represented as particles or individuals within a swarm or population. Initially, the population of particles is randomly initialized [33]. These particles traverse a multidimensional search space, communicating with each other to explore and exploit the search area effectively. Each particle navigates towards its own best-known position (self-cognition or **pbest**) and the overall best-known position across the population (social cognition or **gbest**).

The movement of particles is governed by three main components: a control parameter, the self-cognition component, and the social cognition component. The **pbest** represents the best position a particle has achieved individually, while **gbest** denotes the best position found by any particle in the entire swarm. At each iteration t, particles update their velocity $\mathbf{v}_p^t$ and position $\mathbf{x}_p^t$ using equations 3a and 3b [34], respectively.

$$\mathbf{v}_p^{t+1} = w\mathbf{v}_p^t + c_1 r_1^t \left[\mathbf{pbest}_p^t - \mathbf{x}_p^t\right] + c_2 r_2^t \left[\mathbf{gbest}^t - \mathbf{x}_p^t\right] \tag{3a}$$

$$\mathbf{x}_p^{t+1} = \mathbf{x}_p^t + \mathbf{v}_p^{t+1} \tag{3b}$$

The term w represents the inertia weight or control parameter in the PSO algorithm. The coefficient c_1 denotes the local best acceleration coefficient or autocognitive constant, while c_2 refers to the global best acceleration coefficient or social constant. These constants regulate the balance between exploitation (local best) and exploration (global best) within the search space. During each iteration, random values r_1 and r_2 are generated between 0 and 1.

The local best position $\mathbf{pbest}_p$ for each ASV p is computed using Eq. 4a, where $\mathbf{x} \in \mathcal{U}_{(p)}$ represents the coordinates that ASV p has visited. Here, $\mathcal{U}_{(p)}$ denotes the set of points traversed by ASV p.

To determine the global best position **gbest**, Eq. 4b is applied, considering all coordinates visited by the entire fleet, denoted by $\mathbf{x} \in \mathcal{U}$. Here, $\mathcal{U}$ represents the set of all coordinates visited by the fleet.

$$\mathbf{pbest}_p^t = argmax\{\mu(\mathbf{x})\} : \mathbf{x} \in \mathcal{U}_{(p)} \tag{4a}$$

$$\mathbf{gbest}^t = argmax\{\mu(\mathbf{x})\} : \mathbf{x} \in \mathcal{U} \tag{4b}$$

4.2. Enhanced GP-based PSO

This approach represents an enhanced version of the PSO path planner incorporating GP for surrogate modeling [13]. The movement is guided by four key components: local best, global best, GP mean, and GP uncertainty. The principal elements of the Enhanced GP-based PSO are detailed below.

4.2.1. Gaussian Process

The GP is a stochastic process based on Bayesian inference [35][36]. The input to the GP consists of a data set with inputs considered as random

variables. The GP is completely defined by two components: the covariance function or kernel and the mean function [36]. Nevertheless, the mean function is usually zero. For this informative path planning, the mean function is zero, so the component that defines the GP behavior in this algorithm is the kernel function. The kernel function specifies the smoothness, variability, and shape of the model of the water quality parameters of the water resource. According to the results obtained in [14], the Radial Basis Function (RBF) has the best behavior for water resources. The RBF kernel depends on a single hyper-parameter named length-scale ℓ, which controls the covariance in terms of the distance between measurements performed.

To update the Gaussian Process Regression (GPR), the input data, $\mathcal{D}$, is conditioned and marginalized. Eq. 5 is used to calculate the unknown response, where $\mu(\mathbf{x}_*)$ is the mean value and $\sigma(\mathbf{x}_*)$ is the standard deviation of the GPR $\hat{y}(\mathbf{x})_*$.

$$\mu_{\hat{y}(\mathbf{x}_i)_*|\mathcal{D}} = K_*^T(K + \sigma_o^2)^{-1}y(\mathbf{x}) \tag{5a}$$
$$\sigma_{\hat{y}(\mathbf{x}_i)_*|\mathcal{D}} = K_{**} - K_*^T(K + \sigma_o^2)^{-1}K_* \tag{5b}$$

where the term σ_o refers to expected measurement noise. Measurement noise allows a better adjustment of water quality measurements, since GPs consider these values [22]. The terms K, K_{**} and K_* are data from the fitted kernel. These variables include covariances between known data $k(\mathbf{x}, \mathbf{x})$, unknown data $k(\mathbf{x}*, \mathbf{x}*)$, and covariances between both, the known and unknown data $k(\mathbf{x}, \mathbf{x}*)/k(\mathbf{x}*, \mathbf{x})$.

$$K = \begin{bmatrix} K & K_* \\ K_*^T & K_{**} \end{bmatrix} = \begin{bmatrix} k(\mathbf{x}, \mathbf{x}) & k(\mathbf{x}, \mathbf{x}*) \\ k(\mathbf{x}*, \mathbf{x}) & k(\mathbf{x}*, \mathbf{x}*) \end{bmatrix} \tag{6}$$

With an appropriate selection of a kernel function, GPs can efficiently approximate a real unknown behavior $y(\mathbf{x})$. Therefore, the value at any location $\mathbf{x}$ can be approximated. Ultimately, the approximated values can help the PSO-based system to execute better behaviors.

4.2.2. Path Planner

The Enhanced GP-based PSO integrates elements from both PSO and GP for path planning. It combines the PSO components, the local best **pbest**

and global best **gbest**, with data derived from GP modeling, specifically the uncertainty σ and the mean μ. The term μ represents the estimated pollution data of water resources.

The algorithm starts by collecting water quality measurements using sensors deployed in the water resource. These measurements are used to update the GP model. Subsequently, leveraging the updated model of the GP, the path planner computes the maximum values of uncertainty and mean to adjust the velocity and position of ASVs using Eq. 7.

$$\mathbf{v}_p^{t+1} = w\mathbf{v}_p^t + c_1 r_1^t[\mathbf{pbest}_p^t - \mathbf{x}_p^t] + c_2 r_2^t[\mathbf{gbest}^t - \mathbf{x}_p^t] + c_3 r_3^t[\mathbf{max\_un}^t - \mathbf{x}_p^t] + c_4 r_4^t[\mathbf{max\_con}^t - \mathbf{x}_p^t] \tag{7a}$$

$$\mathbf{x}_p^{t+1} = \mathbf{x}_p^t + \mathbf{v}_p^{t+1} \tag{7b}$$

The velocity $\mathbf{v}^{t+1}$ is obtained as the sum of the velocity $\mathbf{v}^t$ and contributions from the surrogate model and PSO components. The term w represents the inertia weight. The surrogate model data is denoted by $\mathbf{max\_un}^t$ and $\mathbf{max\_con}^t$. $\mathbf{max\_un}^t$ identifies the coordinate where the maximum model uncertainty value $max\sigma^t$ occurs, as shown in Eq. 8a. Conversely, $\mathbf{max\_con}^t$ indicates the coordinate with the maximum model mean value $max\mu^t$, which relates to the maximum contamination of the water resource, according to Eq. 8b. To compute these, all available coordinates $\mathbf{x}$ in the search space $\mathcal{N}$ are considered. The coefficients c_1, c_2, c_3, and c_4 are acceleration coefficients that determine the importance of each term; higher values indicate greater importance. c_1 and c_4 emphasize exploitation, while c_2 and c_3 emphasize exploration. The position $\mathbf{x}^{t+1}$ is updated by adding the velocity $\mathbf{v}^{t+1}$ to the current position $\mathbf{x}^t$. r_3 and r_4 represent random values in the range [0, 1].

$$\mathbf{max\_un}^t = argmax\{\sigma(\mathbf{x})\} : \mathbf{x} \in \mathcal{N} \tag{8a}$$

$$\mathbf{max\_con}^t = argmax\{\mu(\mathbf{x})\} : \mathbf{x} \in \mathcal{N} \tag{8b}$$

Measurements of the water quality parameters are not taken at each iteration of the algorithm to avoid collecting excessive data, which would prolong the GP adjustment process. Instead, a condition based on distance is used to trigger measurements, as described in Eq. 9 [14]. Specifically, if the distance between the current position of the ASV $\mathbf{x}^t$ and the position where the

last measurement was taken $\mathbf{x}_{measure}$ exceeds a threshold distance l, then a measurement of the physico-chemical parameters is conducted.

$$l = \lambda \times \ell^t \tag{9}$$

The term λ refers to the ratio of the length scale, and the term ℓ^t represents the posterior length scale of the GP.

4.3. Enhanced GP-based PSO based on Epsilon Greedy method

This is an improved version of PSO that incorporates both exploration and exploitation phases using the epsilon-greedy methodology, commonly employed in DRL [21, 37]. In the Enhanced GP-based PSO, applying the epsilon-greedy method allows the algorithm to dynamically adjust its focus during the monitoring task. This is facilitated by the epsilon function ϵ, which probabilistically modifies the values of the acceleration coefficients (c_1, c_2, c_3, and c_4) in the Enhanced GP-based PSO, thereby controlling the trade-off between exploration and exploitation.

Initially, the initial combination of acceleration coefficient values for exploration ($Explore$) and exploitation ($Exploit$) is selected. During algorithm execution, the probability that ASVs engage in surface exploration is 95%, as epsilon ϵ is set to 0.95. As ASVs travel a distance $d\epsilon_0$, epsilon ϵ starts decreasing by $\Delta\epsilon$. This decrement continues until ASVs reach a traveled distance of $d\epsilon_f$. At this point, epsilon ϵ remains constant again but at 0.05, indicating a 5% probability to explore the water resource surface, prioritizing exploitation of contamination zones.

The condition determining whether the algorithm focuses on exploration or exploitation is based on the relationship between epsilon ϵ and a random number val, generated at each iteration. If epsilon ϵ is greater than val, ASVs focus on surface exploration; if epsilon ϵ is less than val, ASVs concentrate on exploiting contamination zones. Once coefficients are determined, the path planner operates like the Enhanced GP-based PSO, using GP mean and uncertainty to update the positions and velocities of ASVs via Eq. 7.

Algorithm 1: Enhanced GP-based PSO based on Epsilon Greedy method pseudo-code.

$\mathbf{x}_p^0 \leftarrow$ Initialize PSO; `// where` $\mathbf{x}^0$ `is the initial position of the ASV` p
while *not done* **do**
  if $dist_{total} \leq d\epsilon_0$ **then**
    $\epsilon^t \leftarrow 0.95$
  else if $dist_{total} \geq d\epsilon_f$ **then**
    $\epsilon^t \leftarrow 0.05$
  else
    $\epsilon^t \leftarrow \epsilon^{t-1} - \Delta\epsilon$
  $val \leftarrow random()$;
  if $\epsilon^t \geq val$ **then**
    $c_1, c_2, c_3, c_4 \leftarrow$ Explore
  else
    $c_1, c_2, c_3, c_4 \leftarrow$ Exploit
  $\mathbf{pbest}_p,\ \mathbf{gbest} \leftarrow$ Evaluate fitness function;
  $dist \leftarrow \mathbf{x}^t - \mathbf{x}_{measure} \leftarrow$ Calculate distance;
  if $dist \geq l$ **then**
    $m \leftarrow$ Take measurements;
    $\sigma_s^t,\ \mu_s^t \leftarrow$ Adjust GP;
    $max\sigma_s^t,\ max\mu_s^t \leftarrow$ Find maximum values;
    $\mathbf{max\_un}^t,\ \mathbf{max\_con}^t \leftarrow$ Obtain coordinates of the maximum values;
  $\mathbf{v}_p^{t+1},\ \mathbf{x}_p^{t+1} \leftarrow$ Update speed and position of the ASVs;

5. Proposed informative path planning: AquaFeL-PSO

The main objective of this section is to develop an informative path planner based on a multi-modal PSO [33], GP [36], and FL paradigm [38, 39, 40, 41]. This new informative path planner builds on the Enhanced GP-based PSO [13] (Section 4.2), incorporating enhancements to increase precision and accuracy in detecting and monitoring areas with high contamination. The key improvement involves dividing the informative path planner into two phases: exploration and exploitation. Evaluations with different PSO-based algorithms have demonstrated that optimal results are achieved by shifting

focus during the monitoring task [42]. Unlike the epsilon-greedy method (Section 4.3), this new informative path planner employs controlled periods for phase transitions. The change between phases is managed by controlling the distance traveled by the vehicles, rather than relying on a random variable.

Algorithm 2 presents the pseudocode of the proposed informative path planning, which begins with focusing on the exploration of the surface water resource, referred to as the exploration phase. The goal of this initial phase is to obtain a reliable water quality model to identify the areas of highest contamination within the water resource, known as action zones. When the distance traveled by the ASVs ($asv\_distance$) reaches a predetermined value, called the exploration distance ($exploration\_distance$), the estimated water quality model is derived from the measurements taken during the exploration phase. Once this model is established, the system transitions to the exploitation phase. During the exploitation phase, measurements of the water quality parameters are concentrated in the areas with the highest detected contamination levels. In this phase, the surface of the water resource is divided into action zones ($\mathcal{A}$), and the ASVs are assigned to these zones ($\mathcal{P}_{(a)}$). The decision and assignment of ASVs occur only once, based on the proximity of the ASV to the center of the action zone. Once assigned, the ASVs move directly to their designated action zones to exploit them, enhancing the model. Each action zone maintains its own estimated model, starting from the model obtained in the exploration phase. The monitoring task concludes when the ASVs reach a traveled distance equal to the exploitation distance ($exploitation\_distance$). Finally, the estimated models from each action zone are merged to produce a single water quality model of the entire water resource. The values of exploration distance and exploitation distance are parameters set at the beginning of the algorithm.

Algorithm 2: Proposed informative path planning pseudocode

$\mathbf{x}_p^0 \leftarrow$ Initialize PSO; `// where` $\mathbf{x}^0$ `is the initial position of the ASV` p.
while *not done* **do**
  while *asv_distance* $\leq$ *exploration_distance;* `// Exploration phase` **do**
    $\mathbf{v}_p^{t+1}$, $\mathbf{x}_p^{t+1}$ * $\leftarrow$ Update speed and position of the ASVs using Eq. 10 and Eq. 7b.
  $\mathcal{A} \leftarrow$ Obtain action zones for the water quality parameters.
  $\mathcal{P}_{(a)} \leftarrow$ Assign vehicles to the action zones.
  while *asv_distance* $\leq$ *exploitation_distance;* `// Exploitation phase` **do**
    $\mathbf{v}_p^{t+1}$, $\mathbf{x}_p^{t+1}$ * $\leftarrow$ Update speed and position of the ASVs using Eq. 13 and Eq. 7b.

*The term $\mathbf{v}_p^{t+1}$ represents the velocity of the ASV p at time $(t+1)$, and the term $\mathbf{x}_p^{t+1}$ represents the next position of the ASV p.

5.1. Exploration phase

In this first phase, the ASVs focus on covering and measuring as much of the water resource as possible. The objective is to obtain an initial estimated model of the water quality, which is used later in the exploitation phase to determine the action zones. Without a good mapping of the water resource, it is challenging to identify potential contamination zones. Consequently, it becomes impossible to detect areas of greatest contamination and pollution peaks. An example of the estimated water quality model obtained in this phase can be seen in Fig. 3. During this stage, a centralized learning technique is employed where all measurements taken by the vehicles are sent to the central server, generating a single estimated model. This phase concludes when the vehicles have traveled a predefined distance, at which point the informative path planning shifts its focus to exploitation.

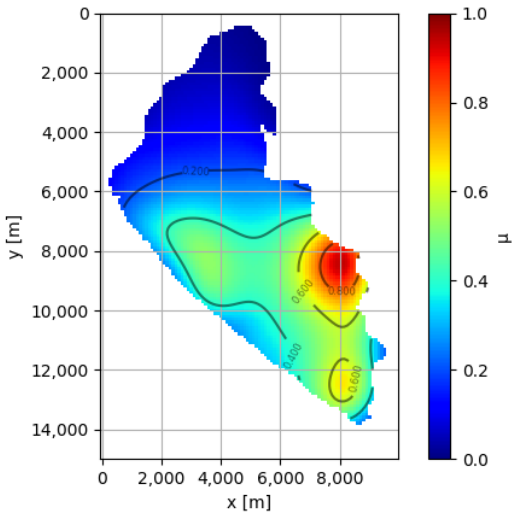

Figure 3: An example of the water quality model obtained in the exploration phase.

Since the proposed informative path planning is based on the Enhanced GP-based PSO, the velocity and position update follows Eq. 7a. In this first phase, the objective of the monitoring task is to obtain a reliable initial estimate of the water quality model of the water resource. Therefore, the active acceleration coefficients are the local best (c_1) and the surrogate model uncertainty (c_3) coefficients, as it has been demonstrated that these coefficients enable the informative path planning to focus on exploring the surface of the water resource [24]. Consequently, the new velocity equation for this phase is given in Eq. 10, while the position is updated using the same equation as the Enhanced GP-based PSO, Eq. 7b.

$$\mathbf{v}_p^{t+1} = w\mathbf{v}_p^t + c_1 r_1^t[\mathbf{pbest}_p^t - \mathbf{x}_p^t + c_3 r_3^t[\mathbf{max\_un}^t - \mathbf{x}_p^t] \tag{10}$$

5.2. Exploitation phase

Once a reliable initial water quality model of the water resource has been obtained in the exploration phase, the exploitation phase uses this information to further characterize the water quality parameters and identify the most polluted areas. The exploitation phase is divided into several stages, each of which is described below.

5.2.1. Action zones

Using the estimated model generated in the exploration phase, areas with high contamination levels are identified. The contamination levels are cate-

gorized as follows: acceptable (0 - 32% contamination, indicated in green), warning (33% - 65% contamination, indicated in yellow), and risk (66% - 100% contamination, indicated in red). The percentage of contamination is determined from the maximum contamination value found in the exploration phase. For example, 33% represents 33% of the maximum contamination value observed during the exploration phase. The purpose of establishing these levels is to create three equally sized ranks, although these may be adjusted based on practical acceptable levels of water quality parameters. Fig. 4 illustrates an example of the estimated model obtained in the exploration phase, taking into account the percentage of contamination. In this work, circular action zones are considered. The peaks of the contamination values from the estimated model obtained in the exploration phase serve as the centers of these action zones.

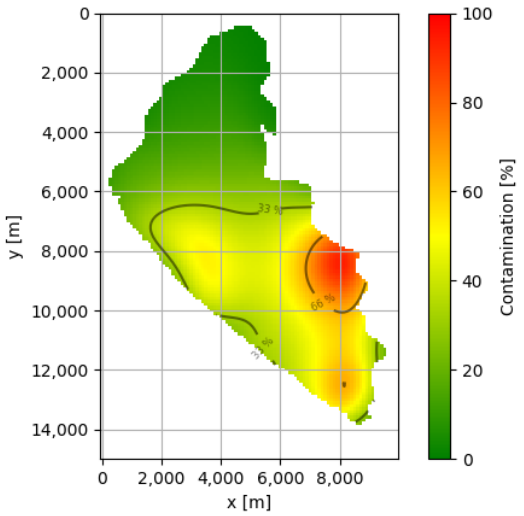

Figure 4: An example of the estimated model taking into account the percentage of contamination.

- **Area of action zones:** To obtain the action zones, a radius of action (rad) is calculated that determines the area covered by vehicles during the exploitation phase. The area of action zones should adapt to the length of water resources, and also, the number of vehicles available for the monitoring mission. Thus, if more vehicles can be used, the resolution of the action zones can be increased by decreasing the area of the action zone. Therefore, the proposed action radius is shown in

Eq. 11, where the radius of action is the value of the side of the shortest perimeter of the lake ($length$) divided by the number of vehicles n_{ASVs} in the ASV fleet.

$$rad = \frac{length}{n_{ASVs}} \tag{11}$$

An important point to note is that the action zones do not overlap. That is, if a map coordinate belongs to an action zone, that coordinate is already discarded when obtaining the following action zones.

- **Number of action zones:** To determine the number of action zones, first a contamination threshold has to be selected; if the contamination value at a certain coordinate is higher than the contamination threshold, that coordinate is considered as a possible action zone center. The selected contamination threshold is 33% of the maximum value of contamination from the exploration phase, since it is considered that below such threshold, water is in optimal condition. Among all coordinates that meet this requirement, the coordinates of the maximum value are considered the center of the first action zone. Then, the procedure is recursive by eliminating the area within the first action zone, and consequently, determining the center of the second action zone among the rest of the water resources that are above the 33% contamination threshold of the exploration phase. The procedure finishes when the maximum number of action zones is determined. The maximum possible number of action zones equals the number of vehicles in the fleet. Notice that between the centers of two action zones, there will never be a distance smaller than the action radius because the center of the action zone is obtained considering the coordinates outside the circumference. As a consequence of the proposed procedure for determining the action zones, two cases can occur: 1) there can be fewer action zones than vehicles, this is because there are fewer pollution peaks than ASVs; 2) there can be the same number of action zones as vehicles, this is because there are the same number of pollution peaks as vehicles. In this work, it is not considered to have more action zones than vehicles, since the number of pollution peaks is limited by the number of vehicles.

5.2.2. Resource allocation

Once the action zones have been obtained, the vehicles are assigned to the action zones with the objective that ASVs exploit the zone. The ASVs are assigned according to the distance between the vehicle and the center of the action zone. The ASV that is closest to the action zone is the one that takes advantage of that zone. In case there are more ASVs than action zones, more than one vehicle is assigned to certain action zones. The priority of the action zone is the condition to determine the assignment of the vehicles in this case. The priority of the action zones is determined by the peak contamination value of the action zone. Thus, the highest priority would be given to the action zone that has the highest peak contamination of the model estimated in the exploration phase. This parameter is used to assign vehicles to action zones in case there are more vehicles than action zones. The higher the priority of the action zone, the higher the probability that there will be more ASVs exploiting the area. The maximum value of the priority max_prt depends on the number of available vehicles in the fleet and is obtained by applying Eq. 12:

$$max\_prt = n_{ASVs} * 10 + 10 \tag{12}$$

where n_{ASVs} is the number of available vehicles. Each time a vehicle is assigned to an action zone, the priority decreases by 10 points.

5.2.3. Exploitation of action zones

After obtaining the action zones and assigning the ASVs, the actual exploitation task is conducted. By dividing the fleet into different action zones, the fleet is divided into sub-populations. Each sub-population focuses on the exploitation of its action zone, hence the maximum contamination and maximum uncertainty data are different for each sub-population, as well as the global best. To calculate the maximum value of each action zone, only the data of the coordinates that are in that action zone are taken into account, discarding the other coordinates of the map. In this way, the exploitation of this action zone is not affected by the other action zones. Moreover, each sub-population calculates a different global best; therefore, the global best of a sub-population is the best position among the vehicles that are in the same action zone. If there is only one vehicle in the action zone, the global best is equal to the local best. To end with the monitoring, the vehicles must travel a certain distance, which is the exploitation distance. As in the

exploration phase, in the exploitation phase, Eq. 7 is used as the basis for updating velocity and position. In this phase, the acceleration coefficients that remain active are the local best (c_1), global best (c_2) and contamination (c_4) coefficients, with higher values for the local best and contamination coefficients. It has been demonstrated in [25], that with this combination, the algorithm exploits the zones through which the ASV passes and the zone with the highest contamination. Therefore, the velocity update equation in the exploitation phase is expressed as Eq. 13, and the position update is performed by applying Eq. 7b.

$$\mathbf{v}_p^{t+1} = w\mathbf{v}_p^t + c_1 r_1^t[\mathbf{pbest}_p^t - \mathbf{x}_p^t] + c_2 r_2^t[\mathbf{gbest}^t - \mathbf{x}_p^t] + c_4 r_4^t[\mathbf{max\_con}^t - \mathbf{x}_p^t] \quad (13)$$

5.2.4. Federated/distributed Learning

In recent years, the Federated Learning (FL) technique has received a lot of attention and many studies have been conducted [43][44][45]. FL is a special category of Distributed Machine Learning (DML) [43]. This technique alleviates the problem of heavy traffic of data in the central server. This is done by using the data collected from the exploration phase to train the GP of the ASVs within the nodes of each action zone in the exploitation phase.

To obtain the estimated water quality model of the water resource, the FL, is applied. The FL technique is a new concept that was introduced by McMahan et al., with the aim of updating language models in cell phones [38][39][40][41]. The idea of the FL is to generate an ensemble ML model [43]. The data that are used to generate this model are scattered in multiple sites. These data are trained by the local servers or nodes, and the information that is shared with the central server is the result of the training across those multiple local servers or nodes. In this way, the security of the data of each node and the privacy of each node are preserved. The final result obtained in the central server is very similar to the final model generated by a system with a centralized learning technique [43]. In addition to promoting the privacy and security of the framework, nodes can train ML models in a collaborative manner, allowing better results to be generated [43][44]. Among the drawbacks of the FL are: the communication between nodes and the central server can be unstable and slow; and the more nodes there are, the more likely the system will become unpredictable and unstable [43][44].

For a better understanding, reference is made to the definition provided by [43]. Consider $\mathcal{L}$ nodes, with the vector of nodes being equal to $\mathbf{F} = \{\mathcal{F}_k \mid k =$

$1, 2, \ldots, \mathcal{L}\}$. In this work, the nodes are the sub-populations or sub-fleets that are created in the Resources allocation stage, discussed in Section 5.2.2 of this article. These nodes train ML models using water quality data obtained from the exploitation of its action zone, $\mathbf{W} = \{\mathcal{D}_k \mid k = 1, 2, \ldots, \mathcal{L}\}$. In the case of a central server, the data of the individual nodes $\mathcal{D} = \mathcal{D}_1 \cup \mathcal{D}_2 \cup ... \cup \mathcal{D}_\mathcal{L}$ would be joined together to obtain a model $\hat{y}_{CEN}$. However, with FL, each node trains its own model $\hat{y}_{FED}$ without exposing the privacy of its data and without being affected by data from other nodes. Moreover, the accuracy of the model generated with the FL $\hat{y}_{FED}$, being the accuracy $\mathcal{V}_{FED}$, is quite close to the model generated with the central server $\hat{y}_{CEN}$, $\mathcal{V}_{CEN}$. That is, considering δ a non-negative real number, if

$$|\mathcal{V}_{FED} - \mathcal{V}_{CEN}| < \delta \tag{14}$$

Then, the federated learning algorithm suffers a loss of accuracy δ.

Having clarified the definition of FL, the FL technique in the proposed informative path planning is explained. Fig. 5 shows the FL-based process. The sub-population of ASVs assigned to an action zone forms a node in the FL technique. For each action zone, a different estimated model is generated, considering the previous data from the exploration phase and the new data collected by the vehicles in that zone. Therefore, the generation of the action zone models is performed at each node. For the final water resources model, the results obtained in each node during the exploitation phase will replace those of the first model obtained in the exploration phase in the central server. The data to be replaced from the model obtained in the exploration phase are the mean and uncertainty values. These values are replaced by the new models generated from the corresponding action zones during the exploitation phase.

FL allows the action zone model generated at its node to not affect the generation of the other action zone models. When using the FL technique, each node has a different GP configuration, i.e., different length scale values. As a consequence, the GP is appropriately adjusted to the measured data to generate the water quality model of each action zone. In case the GP is not able to generate a water quality model of a certain action zone, this does not affect the generation of the models in the other nodes. In these cases, the final model is obtained by keeping the model generated in the exploration phase of the action zone that the GP was not able to generate the model and replacing the zones where a water quality model was obtained.

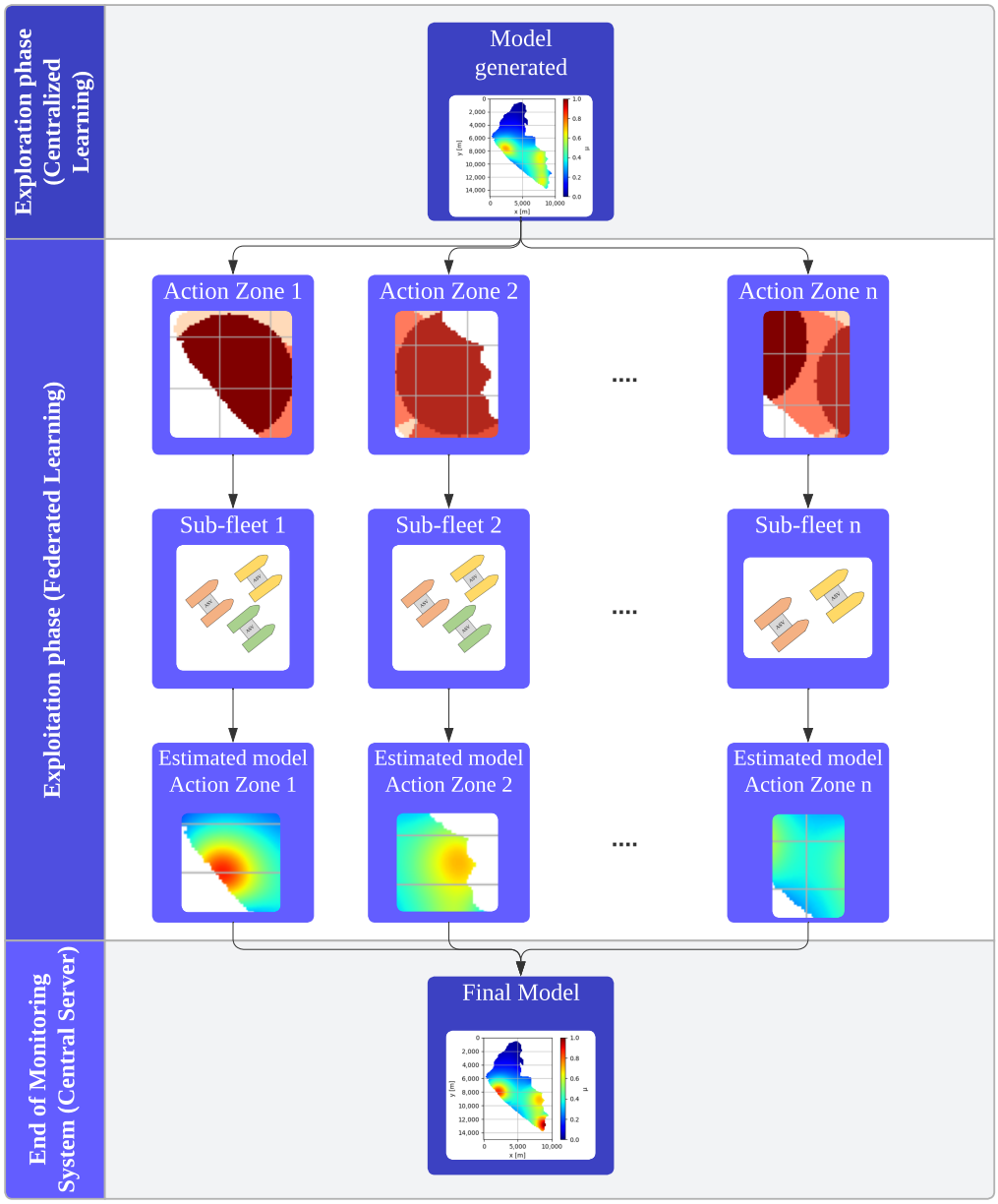

Figure 5: Process based on Federated Learning.

This advantage of FL application is detailed in [46], which examines the performance of the AquaFeL-PSO across various scenarios.

6. Simulation Results

This section contains the performance evaluation of the proposed informative path planning. First, the main simulation parameters used are described, including the Ypacarai lake target scenario, the performance metrics used for evaluation, and the values of the coefficients used in the proposed algorithm. Second, we conduct several analysis to validate the proposed approach in terms of the scalability and duration of the exploration and exploitation phases. Finally, the proposed approach is compared with other contemporary works available in the literature.

6.1. Simulation settings

The code was developed in Python 3.8 using the Scikit-learn[3], DEAP[4] and Bayesian Optimization[5] libraries. The code is available online at Github[6]. The simulations were carried out on a laptop computer with 8GB RAM, Intel i5 1.60 GHz processor.

6.1.1. Simulation environment: Ypacarai Lake

Simulations are conducted using the Ypacarai Lake as the simulation environment. Each element of the map matrix has a dimension of 100 x 100 meters. The distribution map of water quality parameters, or ground truth, is derived from a multi-modal, multi-dimensional, continuous, and deterministic benchmark function: the Shekel function, given by Eq. 15.

$$y_{\text{Shekel}}(\mathbf{x}) = \sum_{i=1}^{R} \frac{1}{c_i + \sum_{j=1}^{Z} (x_j - g_{ij})^2} \tag{15}$$

The Shekel function, being multi-modal, allows for several maximum points, which represent the highest levels of contamination in Ypacarai lake. Examples of the Shekel function applied to the Ypacarai lake scenario are

[3]https://scikit-learn.org/stable/ (accessed on 12 July 2024)
[4]https://deap.readthedocs.io/en/master/ (accessed on 12 July 2024)
[5]https://github.com/fmfn/BayesianOptimization (accessed on 12 July 2024)
[6]https://github.com/MicaelaTenKathen/AquaFeL-PSO.git (accessed on 12 July 2024)

shown in Fig. 6. The Shekel function consists of two components: the positions of the maxima, g_{ij}, and the inverse of the significant values of the maxima, c_i. The positions g_{ij} are contained in matrix G, while the values c_i are in matrix C. Matrix G has dimensions $R \times Z$, where R is the number of maxima and Z is the dimensionality of the space. Matrix C has dimensions $R \times 1$.

The simulations of the algorithms to be compared are performed using 10 different maps generated by the Shekel function. The number of peaks R varies between 2 and the number of vehicles, ensuring the ground truth is multi-modal with more than one peak and aligning with the constraint that the number of action zones should not exceed the number of vehicles, as discussed in Section 5.2.1. The dimensionality of the space Z is 2, representing x and y coordinates. The values of matrix C are generated randomly.

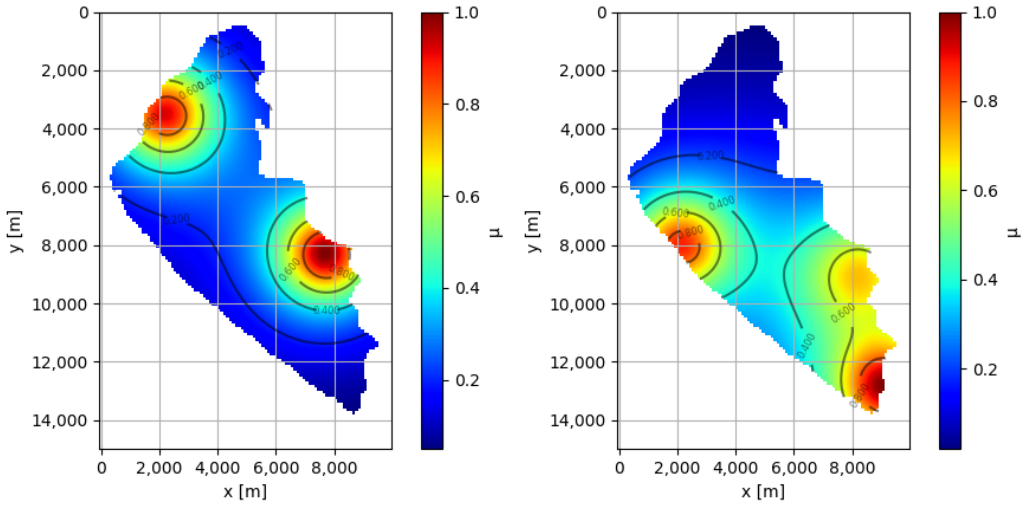

Figure 6: Examples of the actual water quality model of the water resource.

6.1.1.1. Normalization of Data. Since the values of the matrix C in Eq. 15 are obtained randomly, the range of values for the water quality parameters in each ground truth varies. To standardize these values between 0 and 1, normalization is applied to the Shekel function data, as shown in Eq. 16.

$$y_{\text{Normalized}}(\mathbf{x}) = y(\mathbf{x}) = \frac{y_{\text{Shekel}}(\mathbf{x}) - y_{\text{min\_Shekel}}(\mathbf{x})}{y_{\text{max\_Shekel}}(\mathbf{x}) - y_{\text{min\_Shekel}}(\mathbf{x})} \tag{16}$$

In this equation, $y_{\text{Shekel}}(\mathbf{x})$ represents the current value of the function, $y_{\text{max\_Shekel}}(\mathbf{x})$ is the maximum value of the Shekel function, and $y_{\text{min\_Shekel}}(\mathbf{x})$ is the minimum value of the Shekel function.

6.1.2. Performance metrics

The results that are compared between the path planners are the results obtained with the estimated model of the whole lake, the estimated model in the action zones, and the value obtained for the peaks of each action zone. For this purpose, the metrics used are the MSE for the estimated models; and the error between two points, for the value of the peaks of each action zone. The MSE has been selected because this metric is often used to analyze the results of regression models [8]. To calculate the MSE of the entire lake, Eq. 2 in Section 3 is used.

For the MSE of the action zones and the error in the maximum peaks, the action zones of the ground truth were considered. In other words, the division of the map into action zones was applied to the ground truth, since the ground truth is considered as the real model of the water quality of the Ypacarai lake. From these real action zones, the maximum peaks of real contamination were obtained. Then, the MSE and error were calculated taking into consideration the coordinates of the real contamination peaks and real contamination zones.

Besides the main objective, another objective of the proposed informative path planner is to exploit the action zone and obtain the most accurate possible model of that zone, which represents a water resource contamination zone. For this purpose, Eq. 17 is applied:

$$\text{MSE}_{\mathcal{A}}(y(\mathbf{x}), \hat{y}(\mathbf{x})) = \frac{1}{A} \sum_{k=0}^{A-1} (y(\mathbf{x}_k) - \hat{y}(\mathbf{x}_k))^2 \tag{17}$$

where $y(\mathbf{x})$ represents the ground truth values in the action zones and $\hat{y}(\mathbf{x})$ represents the estimated model in the action zone. The term A represents the number of action zones.

Finally, the last objective is to detect the peaks of the action zones. To evaluate the performance of the path planners, Eq. 18 is applied. The error is calculated between the peak value of the ground truth action zone $y(\mathbf{x}_{\text{peak}})$ and the peak value of the ground truth action zone obtained in the generated model $\hat{y}(\mathbf{x}_{\text{peak}})$. When there is more than one action zone, the average of the errors made in the peak of the action zones is calculated. In other words, the

error committed at the peak of each action zone is calculated first. Then, the average of all these errors is obtained.

$$\text{Error}_{\text{peak}}(y(\mathbf{x}), \hat{y}(\mathbf{x})) = \frac{1}{A}\sum_{k=0}^{A-1}(|y(\mathbf{x}_{\text{peak}}) - \hat{y}(\mathbf{x}_{\text{peak}})|) \tag{18}$$

Analysis of variance (ANOVA) is a statistical method used to examine how different factors or combinations of factors influence the mean value of a variable. Its purpose is to compare the means of multiple groups of data to determine if there is a significant difference between them [47]. One-way ANOVA is the simplest form of ANOVA. This technique is used when there is only one independent variable or factor and assesses whether there is a notable distinction between the means of two or more groups. The P-value (p_value) is a numerical representation of the probability that a given set of observations would have been discovered if the null hypothesis were true [48]. The results are considered statistically significant if the P-value is less than the significance level and is considered to reject the null hypothesis. Applying this concept to the comparison metric in this paper, if this P value is less than or equal to 0.05 (5%), there is a significant difference between the data from the compared algorithms:

$$p\_value \leq 0.05 \tag{19}$$

Another data obtained by the ANOVA test, is the distribution created by the variance ratios known as the F distribution (f_value), Eq. 20. To obtain a conclusion, the calculated F value should be compared with a critical F ($f\_critical$) value at an error level α of 0.05 in the F table that can be found in [49]. When comparing the F values, if the calculated F value is greater than the critical F value, it means that there is a significant difference between the means of the data sets. In other words, rejecting the null hypothesis that all data sets have the same mean means that at least one set differs from the rest [49].

$$f\_value = \frac{MSB}{MSW} = \frac{variance\ between\ groups}{variance\ within\ groups} \tag{20}$$

6.1.3. Simulation parameters

The maximum speed at which vehicles can reach is 2 meters per second. The initial positions of the vehicles were selected according to ports or easily

accessible locations around these areas. The coordinates of the initial positions are referenced to the map frame used for the simulations. The ASVs depart from different cities: to the east is San Bernardino, to the south the city of Ypacarai, to the west Aregua and Itaugua, and to the northwest Luque. The value of the length scale of the GP is set to 10, following the recommendation in [8], where it is suggested that a good smoothness is achieved with a length scale of 10% of the value of the search map. Considering the findings in [14] and [13], the range for λ to achieve good performance in informative path planning is set to [0.1, 0.5]. By choosing $\lambda = 0.1$, the ASVs will take more measurements, but the execution time will be longer. Conversely, setting $\lambda = 0.5$ will reduce the time taken, but decrease the number of measurements. To balance these factors, λ is set to 0.3, the midpoint of the range [24].

The values of the acceleration coefficients differ between the exploration and exploitation phases. In the exploration phase, the coefficients are set based on findings in [24], while in the exploitation phase, coefficients from [25] are used. These studies analyzed the behavior of the algorithm in exploration and exploitation, respectively. The acceleration coefficients used are shown in Table 1. These values are applied uniformly across all fleet sizes.

Table 1: Values of the acceleration coefficients for exploration and exploitation phases

Hyper-parameter	Exploration phase	Exploitation phase
c_1	2.0187	3.6845
c_2	0	1.5614
c_3	3.2697	0
c_4	0	3.1262

6.2. Proposed approach evaluation

In this subsection, different tests are carried out to evaluate the proposed informative path planning.

6.2.1. Action zone scalability and resource allocation

Firstly, the evaluation of the scalability of the proposed approach related to the action zones is studied. Fig. 7 shows examples for different numbers of vehicles. The figures on the left display the models obtained in the exploration phase, while the figures on the right illustrate the division of the water resource map into action zones depending on the number of ASVs in the fleet.

This configuration allows for more vehicles and smaller action zones, dividing the polluted areas of the water resource into more zones where more vehicles can exploit different pollution areas, as shown in Fig. 7h.

Table 2 shows the radius rad and maximum priority max_prt parameters of the action zones for each number of vehicles n_{ASVs}. These results were obtained using Eq. 11 and Eq. 12 respectively. The parameter $length$ in Eq. 11 for the Ypacarai lake scenario has a value of 10,000 meters.

Table 2: Parameters of the action zones according to the number of ASVs in the fleet

Number of ASVs	rad [m]	max_prt
2	5,000	30
4	2,500	50
6	1,667	70
8	1,250	90

In Fig. 7, the figures on the right show colors representing the priority of the action zones; the higher the priority, the higher the contamination in that zone. This priority is used for vehicle assignment: if there are more vehicles than action zones, the additional vehicles are assigned to the zones with higher priority.

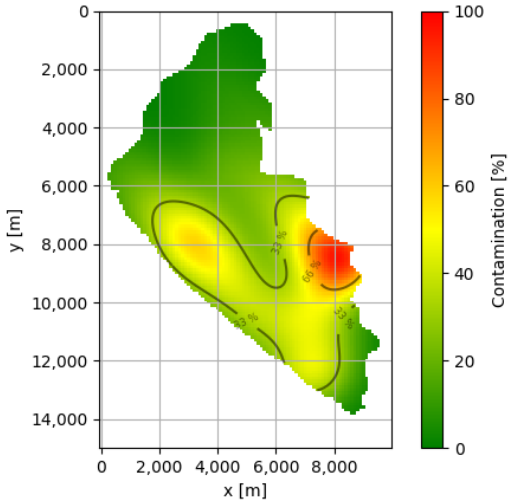

(a) Estimated model obtained on exploration phase with 2 vehicles.

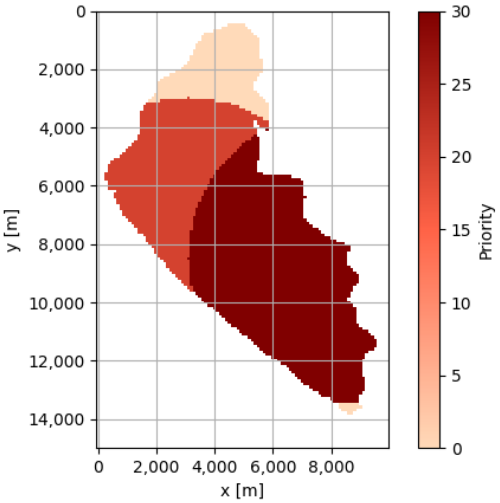

(b) Action zones obtained with 2 vehicles.

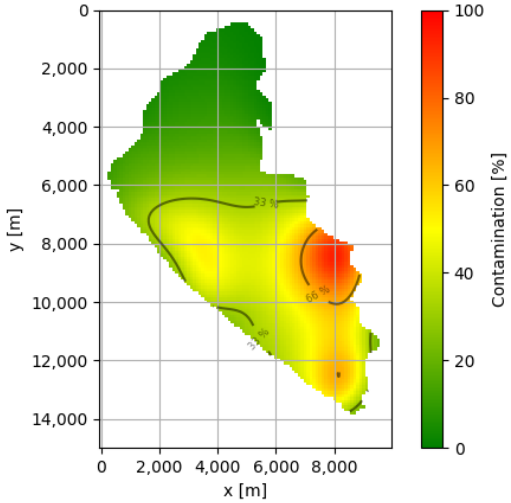

(c) Estimated model obtained on exploration phase with 4 vehicles.

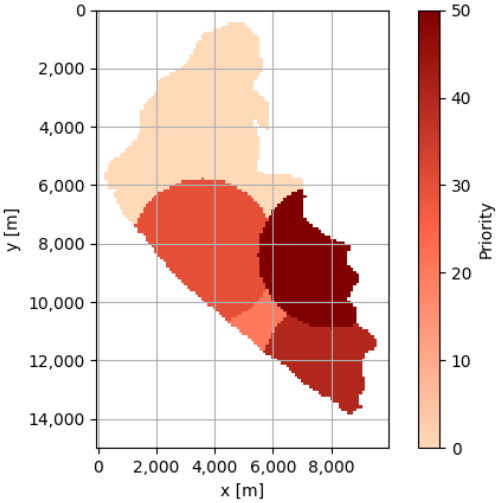

(d) Action zones obtained with 4 vehicles.

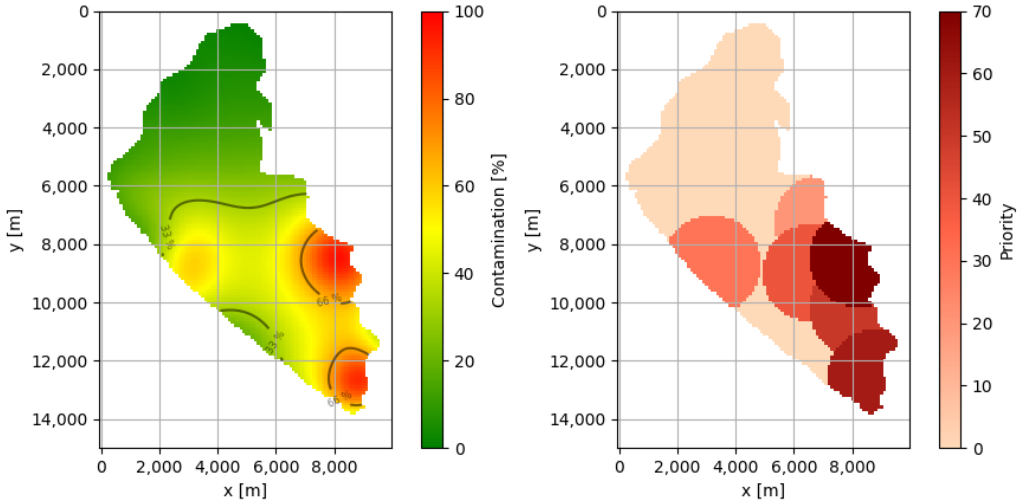

(e) Estimated model obtained on exploration phase with 6 vehicles.

(f) Action zones obtained with 6 vehicles.

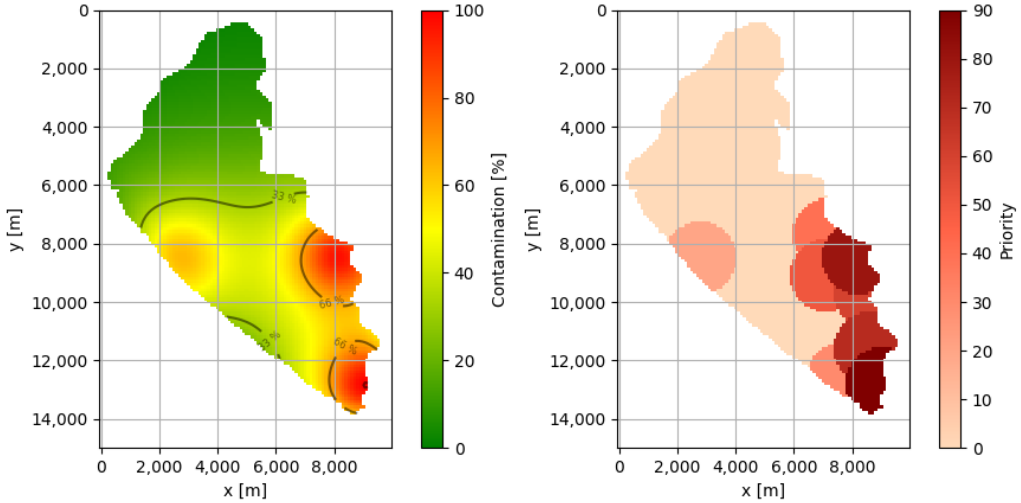

(g) Estimated model obtained on exploration phase with 8 vehicles.

(h) Action zones obtained with 8 vehicles.

Figure 7: Examples of water resource action zones considering the number of ASVs. The figures on the left represent the estimated model obtained in the exploration phase in pollution percentage values, and the figures on the right represent the action zones obtained according to the number of vehicles in the fleet.

6.2.2. Exploration vs Exploitation duration

Before comparing the performance of the proposed approach with that of other path planners, it is essential to determine the optimal combination of

the distance of the exploration and exploitation phases. To achieve this, tests were conducted with several distance combinations for the exploration and exploitation phases. According to Assumption 3 of Section 3, the maximum distance that ASVs can travel is 30,000 meters. Therefore, this maximum distance was used for the tests, with results analyzed for maximum distances of 20,000 meters and 30,000 meters. The tests involved two, four, six, and eight ASVs, with detailed results for two, six, and eight ASVs provided in Section Appendix A. The phase transition distances varied by increments of 5,000 meters (5 km), and the results are presented in kilometers for clarity.

Table 3 shows the mean MSE and confidence intervals for four ASVs at different exploration and exploitation distances when estimating the water quality model across the entire surface water resource. For a maximum travel distance of 20 km, the best combination was found to be 10 km for both exploration and exploitation phases. This indicates that a balanced approach, with 50% of the total distance allocated to exploration and 50% to exploitation, yields the best model. For a maximum distance of 30 km, the optimal combination was 20 km for exploration and 10 km for exploitation. However, the difference between this and the 15 km exploration and 15 km exploitation case was minimal. Thus, it can be concluded that a 50%/50% split between exploration and exploitation is generally optimal, with the possibility of increasing the exploration phase to up to 67% of the maximum distance in some cases. More detailed results for different fleet sizes can be found in Section Appendix A. Fig. 8 graphically represents the results for four vehicles with a maximum distance of 20 km.

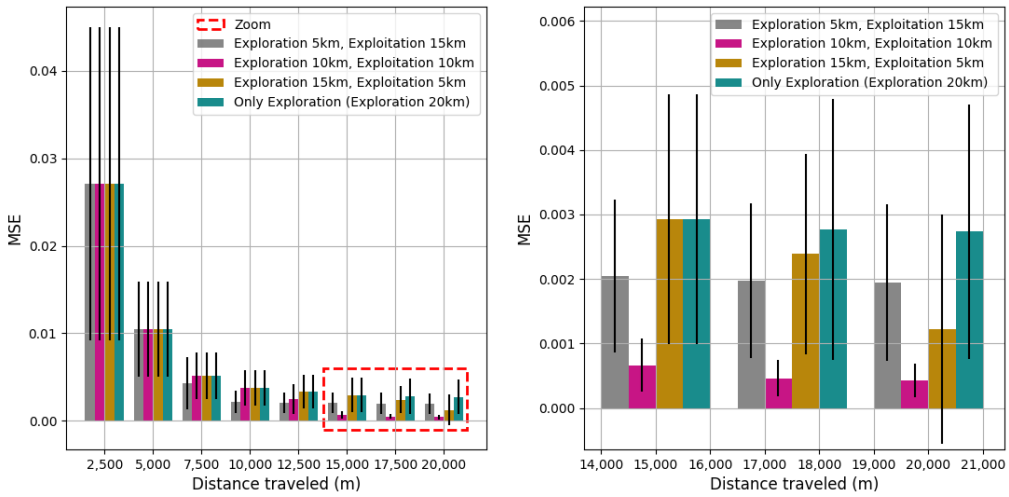

(a) Mean of the MSE with 95% confidence interval of the cases studied for the duration of the exploration and exploitation phases.

(b) Zoom of the mean MSE with 95% confidence interval of the cases highlighted in Fig. 8a

Figure 8: Results obtained from the cases studied for the duration of the exploration and exploitation phases for four ASVs.

Table 3: Comparison between the MSE of the distances traveled in the exploration phase and the exploitation phase for four vehicles

Phase	Distance	MSE 5km	MSE 10km	MSE 15km	MSE 20km	MSE 25km	MSE 30km
Exploration	5km	0.01388 ±	0.0265 ±	0.00217 ±	0.00209 ±	0.00212 ±	0.00195 ±
Exploitation	25km	0.02379	0.00702	0.00462	0.00444	0.00447	0.00459
Exploration	**10km**	0.01388 ±	0.00427 ±	0.00068 ±	**0.00045** ±	0.00045 ±	0.00046 ±
Exploitation	20km	0.02379	0.00509	0.00081	**0.00054**	0.00064	0.00066
Exploration	**15km**	0.01388 ±	0.00427 ±	0.00337 ±	0.00167 ±	0.00032 ±	**0.00029** ±
Exploitation	15km	0.02379	0.00509	0.00467	0.00446	0.00017	**0.00027**
Exploration	**20km**	0.01388 ±	0.00427 ±	0.00337 ±	0.00299 ±	0.00061 ±	**0.00025** ±
Exploitation	10km	0.02379	0.00509	0.00467	0.00418	0.00118	**0.00033**
Exploration	25km	0.01388 ±	0.00427 ±	0.00337 ±	0.00299 ±	0.00169 ±	0.00045 ±
Exploitation	5km	0.02379	0.00509	0.00467	0.00418	0.00138	0.00137
Exploration	30km	0.01388 ±	0.00427 ±	0.00337 ±	0.00299 ±	0.00169 ±	0.00119 ±
		0.02379	0.00509	0.00467	0.00418	0.00138	0.00119

Based on the obtained results, the optimal balance between exploration and exploitation in the AquaFeL-PSO for comparison with other path planners is set at 50%/50%. With a maximum distance of 20 km, this translates to allocating 10 km for exploration and 10 km for exploitation.

Fig. 9 shows the comparison between the model obtained from the action zone in the exploration phase (left), the ground truth (center), and the model

obtained from the action zones in the exploitation phase (right). During the exploration phase, the vehicles traveled 10 km over the surface of the lake. Similarly, in the exploitation phase, the ASVs exploited the contamination zones until they reached a traveled distance of 10 km. This figure demonstrates the improvement of the estimated model in the contamination zones, particularly in action zone 1 (AZ1) and action zone 2 (AZ2). It is important to mention that the action zones created in this test are those shown in Fig. 7d. Additionally, the action zones do not overlap, even though in Fig. 9, the boxes used to indicate the zones may appear to overlap. Each zone is exploited by a single sub-fleet of ASVs.

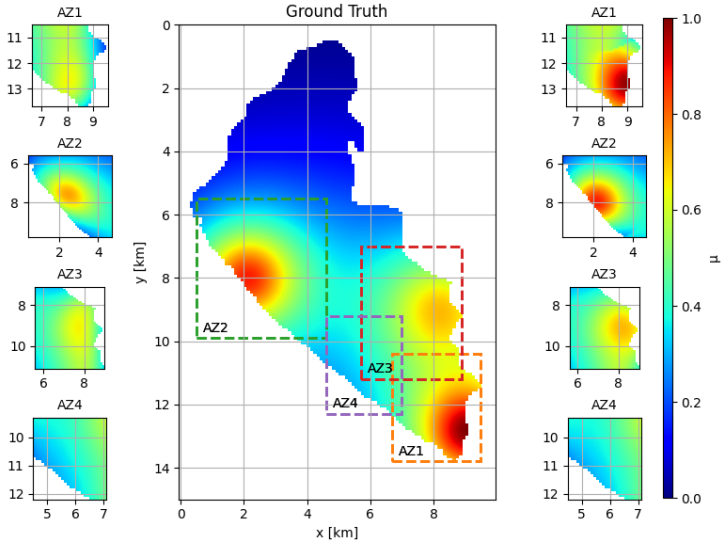

Figure 9: Example of the result obtained with the AquaFeL-PSO informative path planning. The figures on the left show the estimated models of the action zones in the exploration phase, the figure in the center represents the ground truth of the Ypacarai lake, and the figures on the right represent the estimated models of the action zones after the exploitation phase (final model of the action zones).

6.2.3. Centralized vs Federated Learning

This subsection shows the comparison between the application of the FL technique and a centralized learning. Using the centralized learning, the measurements taken by the fleet in the exploitation phase go directly to the main server, and a single estimated water quality model is generated, unlike the FL. The results shown in Table 4 demonstrate that there is very little difference between using a centralized learning or applying the FL technique.

However, as an advantage, with FL, there is no excess data on the central server, since the GP is adjusted at the nodes in each action zone [50]. In addition, the data variability of the system results using the FL technique is lower than the results using the centralized technique.

Table 4: Comparison of MSE and error applying centralized learning and federated learning techniques

Technique	MSE (Action Zones)	Error (Peaks)	MSE (Model of the Lake)	Mean of Time Consuming (sec)
Centralized Learning	0.02304 ± 0.05757	0.00155 ± 0.00985	0.00038 ± 0.00063	8.43176 ± 2.67029
Federated Learning	0.02331 ± 0.05749	0.00160 ± 0.00919	0.00045 ± 0.00055	8.29892 ± 2.22732

6.3. Performance comparison

The performance of the path planners is compared against the lawnmower, random path, random grid path and PSO-based implementations. The algorithms, as presented in [51] are used with necessary adjustments to have a fair comparison.

In the lawnmower, the interspace value corresponds to the length scale of the prior GP. By setting this value, it is ensured that there are no significant changes between the positions where measurements are taken. Additionally, it is expected that the GP model provides significantly different values when the distance is larger than the value of the length-scale.

Random path planners are also compared to the proposed approach: the random waypoints and the random grid path. In these algorithms, the ASVs travel a distance l, Eq. 9, in a given direction, l is the distance that an ASV must travel to take a measurement. When the ASVs travel that distance, random angles are randomly set, which determines the new directions to which the vehicles should go. The difference between the random waypoints and random grid path planners is that in the former, the angles is a number within $[0, 2\pi]$, while, in the second planner, the angles vary discretely between 0 and 2π, in steps of $\pi/2$.

The performance of the AquaFeL-PSO is also compared with the informative path planner based on BO developed in [22], the BO for multiple vehicles. To ensure that the configurations of the algorithms are the same, some changes are made to the BO for multiple vehicles. Firstly, the parameters used in the BO for multiple vehicles, such as grip map, ground truth, distance traveled, among others, are rescaled because the map used in the AquaFeL-PSO has a dimension of 100 x 150, which is smaller than the one

used in [22] (1,000 x 1,500). Secondly, the GP length scale value is also varied to meet this condition: the value of the length scale should be 10% of the value of the search map [8]. Additionally, the GP value is limited in a range of $[1 \times 10^{-10}, 70]$ in order to obtain better water quality models. The ground truths used for the experiments, as well as the initial positions from which the vehicles start, have the same configurations as the AquaFeL-PSO.

For all planners compared, the maximum distance vehicles can travel is 20,000 meters. Therefore, when the vehicles exceed this distance traveled, the monitoring mission ends. The settings for the compared path planners, with respect to water sampling and GP, are the same settings as shown in Section 6.1.3. To set the values of the hyper-parameters in the Classic PSO, [52][53] are taken into consideration, $c_1 = c_2 = 2$. For the Enhanced GP-based PSO (Exploration), the values of the coefficients are the same as those used in the exploration phase [24], Table 1. Moreover, the values of the coefficients used in the Enhanced GP-based PSO (Exploitation) have the same values used in the exploitation phase [25], Table 1. The best combination of parameters for the epsilon greedy method is shown in the Table 5 [42]. Finally, the values of the coefficients for the AquaFeL-PSO algorithm are those shown in the Table 1.

Table 5: Parameter and hyper-parameter values of the Epsilon Greedy method

Parameter/Hyper-parameter	Value
$d\epsilon_0$ (m)	6,500
$d\epsilon_f$ (m)	13,500
$\Delta\epsilon$	0.13
$c_{1explore}$	2.0187
$c_{2explore}$	0
$c_{3explore}$	3.2697
$c_{4explore}$	0
$c_{1exploit}$	3.6845
$c_{2exploit}$	1.5614
$c_{3exploit}$	0
$c_{4exploit}$	3.1262

The comparison of the mean MSE and errors together with the 95% confidence interval is shown in Table 6. The results of the table show that: 1) in the three cases considered (MSE of the action zone, error of the peaks,

and MSE of the whole lake), the proposed AquaFeL-PSO informative path planning has the best performance; 2) the difference between the models obtained from the action zones of the AquaFeL-PSO algorithm and the other path planners is not large, however, in the detection of the peak of each action zone there are large differences, with the random waypoints being the second lowest error, the error obtained with this path planner is more than 40 times greater than the error obtained with the AquaFeL-PSO algorithm; and 3) with respect to the estimated model of the whole lake, the AquaFeL-PSO algorithm has the best MSE and the second best is the MSE of the Enhanced GP-based PSO based on the epsilon greedy method, the difference between the proposed informative path planning and the epsilon greedy method is more than 300%, and the result obtained with the lawn mower algorithm is approximately 7 times greater than the AquaFeL-PSO algorithm.

Table 6: Comparison of MSE and error of the path planners for four vehicles

Path Planner	MSE (Action Zones)	Error (Peaks)	MSE (Model of the Lake)
Lawn mower	0.02957 ± 0.02308	0.13669 ± 0.20769	0.00336 ± 0.00733
Random waypoints	0.02912 ± 0.03231	0.05939 ± 0.14638	0.00361 ± 0.01184
Random grid path	0.03103 ± 0.02218	0.11061 ± 0.26423	0.00638 ± 0.01052
BO for multiple vehicles	0.02719 ± 0.02355	0.20892 ± 0.10825	0.00695 ± 0.00650
Classic PSO	0.03873 ± 0.06193	0.14121 ± 0.22419	0.01146 ± 0.02668
Enhanced GP-based PSO (Exploration)	0.02613 ± 0.02182	0.11632 ± 0.17028	0.00268 ± 0.00368
Enhanced GP-based PSO (Exploitation)	0.04181 ± 0.06892	0.15183 ± 0.22642	0.01266 ± 0.03053
Epsilon Greedy Method	0.02332 ± 0.02783	0.06197 ± 0.11602	0.00184 ± 0.00499
AquaFeL-PSO	**0.02257 ± 0.02631**	**0.00145 ± 0.00380**	**0.00045 ± 0.00052**

Fig. 10 shows the results obtained in Table 6 in graph format. In this boxplot the distribution of the MSE results and errors obtained in the tests can be seen with better precision. The figures show that there is some variability in the results obtained, mainly in the peak error results. This is because in some tests, the ASVs were not able to detect some contamination peaks nor were they able to explore areas where contamination was high. As a consequence, the water quality models were not very accurate. However, there is a significant difference between the dispersion of the AquaFeL-PSO results and the dispersion of the other path planners, the AquaFeL-PSO has much lower data variability than the other algorithms, demonstrating the robustness of the proposed informative path planning. Table 7 shows that in the detection

of contamination peaks in the action zones and in the generation of the water quality model of the lake there is a significant difference between the means of the results, given that the p_value values for both behaviors is less than 0.05 ($p\_value < 0.05$) and that the value of f_value, in both cases, is greater than the value of $f\_critical$ ($f\_value > f\_critical$). In the case of obtaining water quality models of the action zones, there are no significant differences, so the null hypothesis that the means of the path planners are equal is accepted. While modeling the water quality parameters of the action zones may be a task of some importance, it is not as crucial as peak detection and obtaining a water quality model of the entire surface water resource. These latter two tasks are the primary objectives of the proposed approach.

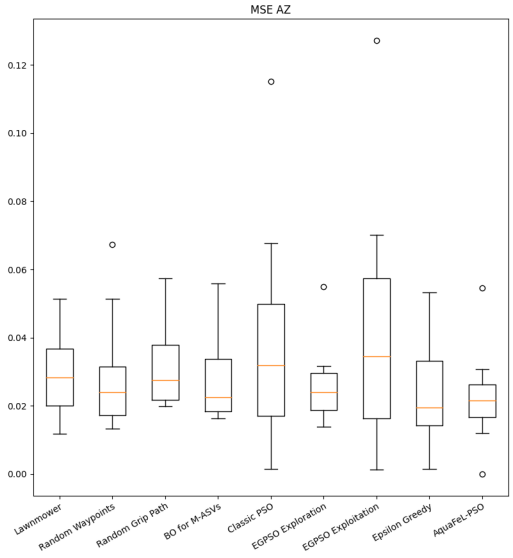

(a) Boxplot of the MSE results of the coordinates of the action zones.

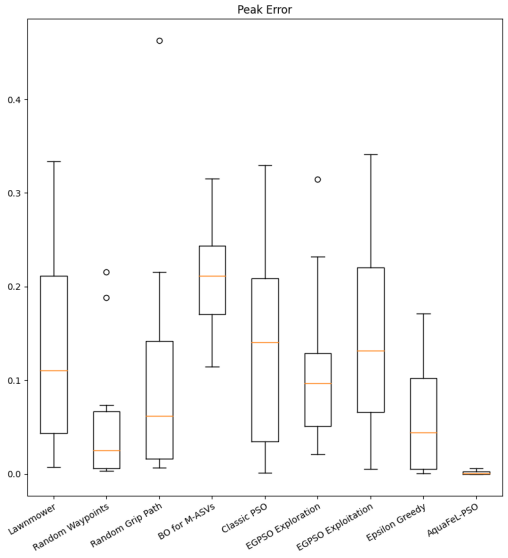

(b) Boxplot of peak error results of action zones.

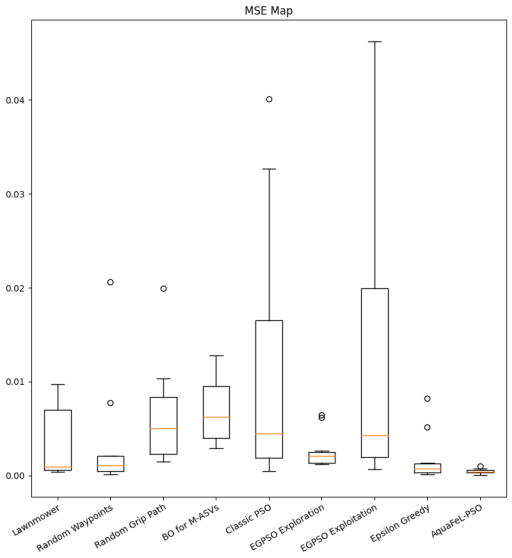

(c) Boxplot of the MSE results of the coordinates of the entire lake.

Figure 10: Representation of the results of Table 6 in boxplot format.

Table 7: Results of the One-way ANOVA test

Performance	p_value	f_value	f_critical
Model of the action zones	0.43757	4.01082	2.05488
Peaks of the action zones	0.00048	1.00682	2.05488
Model of the lake	0.00917	2.77530	2.05488

In Fig 11, the movement of a four-vehicle fleet and the estimated water quality models of the Ypacarai lake can be seen applying different path planners. The graphs at the top show the trajectory performed by the ASVs and the uncertainty of the model. The trajectory of each ASV is represented by a different color. In addition, the initial and final positions of each ASV are indicated by black and red dots, respectively. The graphs at the bottom show the estimated water quality model of the Ypacarai lake. The actual model of this scenario is the ground truth shown in Fig. 6.

Fig. 11a shows how the ASVs move across the surface of the water resource by applying the **Lawn mower path planner**. The vehicles are capable of traversing the entire surface of the water resource allowing the generation of good models of the action zones and an acceptable model of the entire lake. However, the ASVs are not able to exploit the areas of high pollution. As a consequence, the contamination peaks of the action zones are not detected.

In Fig. 11b, the ASVs move according to the trajectories generated by the **random waypoints path planner**. By generating trajectories randomly, the ASVs have the possibility of traversing any area. They are also able to exploit certain areas, since by generating random trajectories, there is a higher probability that vehicles will pass through some areas more than once.

Fig. 11c shows the trajectories generated by the **random grid path planner**. Similar to the previous planner, the paths are randomly generated with the difference that the direction varies in angles multiples of $\pi/2$. By having the angle as a constraint when setting the direction of travel, the ASVs are not able to cover a large area, thus limiting the planner in detecting pollution peaks and obtaining a good model of the lake surface.

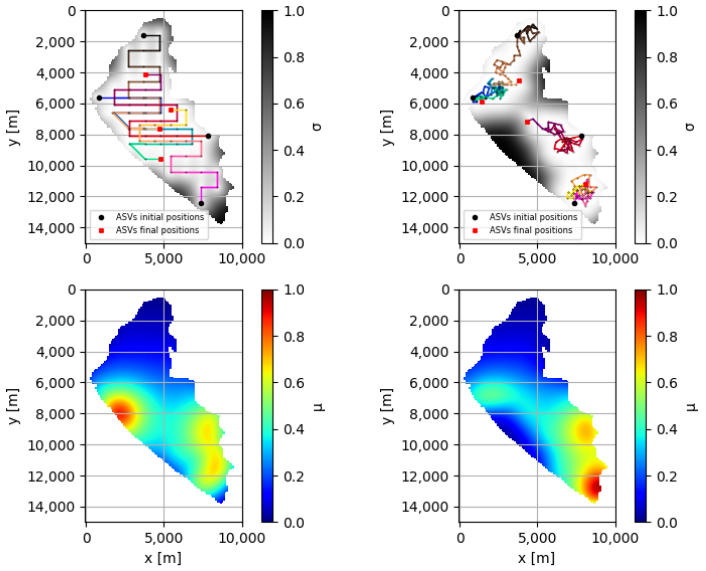

(a) Lawn mower

(b) Random waypoints

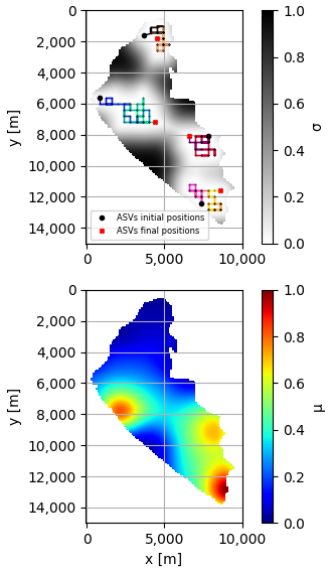

(c) Random grid path

Fig. 11d represents the results obtained with the BO for multiple vehicles. The **BO for multiple vehicles** prioritizes surface exploration of a water resource, aiming to cover as much of the lake as possible. This is reflected in the upper graph of Fig. 11d, which shows a low level of uncertainty in the model, ranging from 0 to 0.3. However, this approach may not effectively

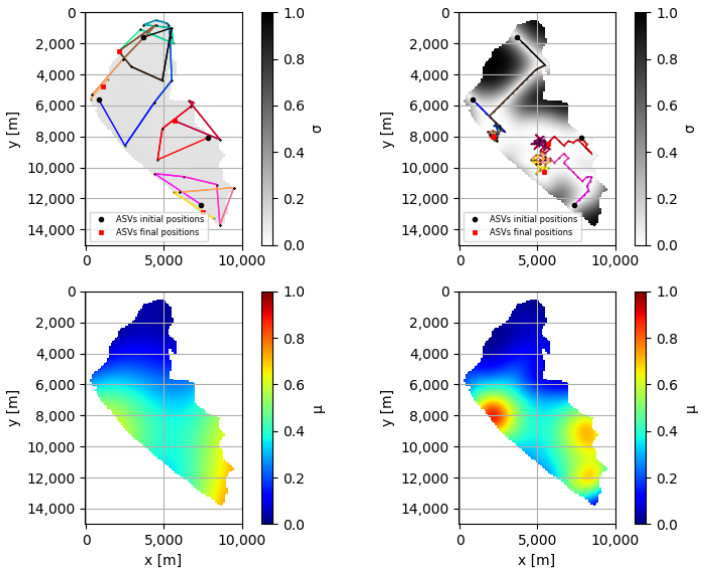

(d) BO for multiple vehicles (e) Classic PSO

address areas with high pollution levels, as the focus is on exploration rather than exploitation. As a result, it may be challenging to thoroughly characterize water quality parameters in heavily polluted areas. The multi-vehicle BO graph the "trajectories" of the ASVs passing over prohibited zones, but in reality, it shows the connection between the target points calculated by the path planner. In case the vehicles encounter an obstacle or forbidden zones, the algorithm uses the a Rapidly-Exploring Random Tree star (RRT*) as a local path planner [8]. The RRT* generates paths that avoid the obstacles or forbidden zones, allowing the vehicles to reach their target points safely.

Fig. 11e represents the trajectories generated by the classical PSO. In the **Classic PSO**, the ASVs are guided by their own experience and by the experience of the other vehicles in the fleet, because of this, after some time, the vehicles are stuck in a local optimum, since they cannot explore the surface anymore. In this scenario, the influence of the global best on the vehicles at the bottom of the lake can be observed, where both vehicles are in contaminated areas. However, as another of the ASVs has found the maximum peak, the global best is the best position of that vehicle, and the ASVs that were at the bottom of the lake, instead of exploiting the area where they are positioned, go to the area where the maximum peak is located.

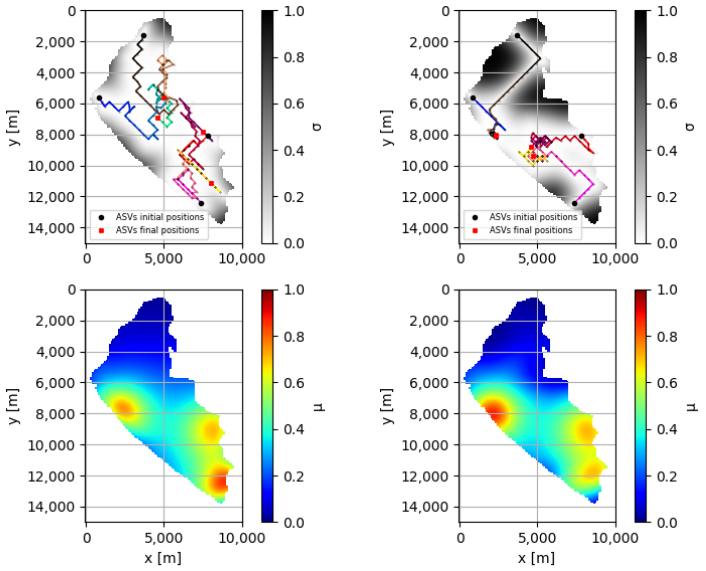

(f) Enhanced GP-based PSO (Exploration)

(g) Enhanced GP-based PSO (Exploitation)

In Fig. 11f, it is shown how ASVs explore the zones where uncertainty is high and are not guided by the zones where contamination is high. This is due to the values of the acceleration coefficients, and the terms that are active are the local best and the maximum uncertainty term. Due to the local best, the vehicles exploit the areas through which they pass, and thanks to the maximum uncertainty, the ASVs go to unexplored areas. This behavior allows to obtain a good water quality model of the water resource. On the other hand, it does not exploit the contamination zones, and as a consequence, a considerable error in the contamination peaks can be obtained.

In contrast to Fig. 11f, in Fig. 11g, the movement of vehicles is shown by applying the **Enhanced GP-based PSO** focused on the exploitation of pollution zones. The active terms in this path planner are the local best, the global best and maximum contamination. Since the ASVs do not explore the surface of the water resource sufficiently, the vehicles are not able to detect all pollution peaks, so the maximum contamination value of the **max_con** term will be determined by the measurements they have taken so far. This means that, when one of the vehicles finds an area with high values, the ASVs will go to that point, whether this is the area where the maximum contamination peak is found or not.

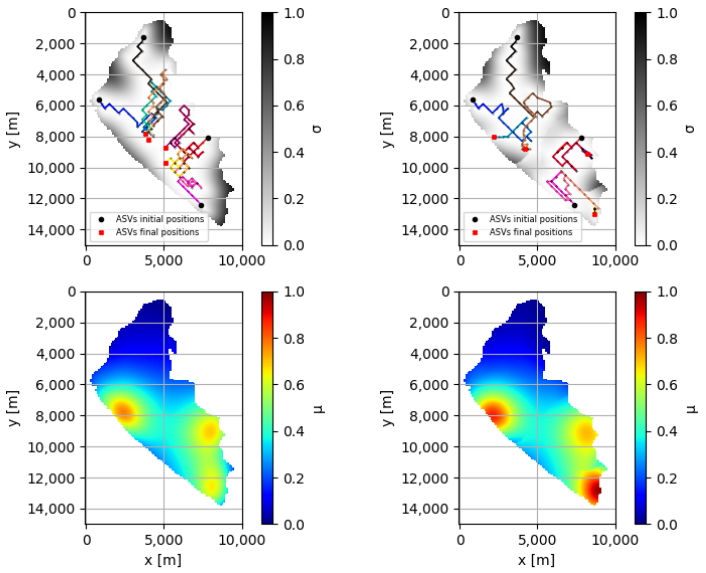

(h) Epsilon Greedy method (i) AquaFeL-PSO

Figure 11: Representation of the results obtained in the monitoring of the Ypacarai lake using 4 vehicles. The graphs at the top represent the movement of the ASVs and the model uncertainty, and the graphs at the bottom represent the estimated water quality model of the lake.

Fig 11h shows the trajectory of the ASVs obtained by applying the **Epsilon Greedy method**, where, during monitoring, the algorithm changes the focus randomly. At the beginning of the monitoring, the probability that the algorithm explores the surface is high. However, as time passes, the probability of exploring the surface decreases and the probability of exploiting contamination zones increases. That can be observed in Fig. 11h, as the ASVs target the area where the generated model estimates the maximum contamination point. As the change of approach is random, there are cases where not enough data are taken to generate a good estimated model, which can affect the detection of contamination zones.

Fig. 11i illustrates the fleet movements applying the proposed informative path planning, the **AquaFeL-PSO**. This system operates in two phases during given periods, dividing the search space into action zones and the fleet into sub-populations, thus providing an accurate model of both the pollution zones and the entire lake. In addition, the path planner is able to detect pollution peaks. After performing the exploration of the lake surface, a model is generated with the obtained measurements, as shown in Fig. 7c.

With this model, the algorithm divides the map into action zones, represented in Fig. 7d. Subsequently, vehicles are assigned to these action zones; in this scenario, each ASV receives a specific zone. During the exploitation phase, the vehicles focus on exploring the contamination zones, obtaining detailed models of each action area. Once this phase is completed, the algorithm replaces the results of the action zones with the estimated model generated during the exploitation phase, thus creating the final water resource quality model, shown in Fig. 11i.

7. Discussion of the Results

The main findings of this work are discussed below:

- Due to the limitations of the PSO algorithm, such as the tendency to fall into a local optimum and the difficulty in setting the initial parameters, improvements must be made in this algorithm to solve multi-modal problems. Based on the results of [24] [25][42], the AquaFeL-PSO is proposed in this work as a solution to multi-modal problems involving water resources monitoring. The AquaFeL-PSO consists of an informative path planning with two phases, with the objective of detecting in the first phase the possible positions of pollution peaks so that in the second phase these areas can be exploited by sub-fleets of ASVs.

- The scalability and vehicle allocation results demonstrated that the proposed informative path planning works effectively with different fleet sizes. In addition, it was verified that the vehicle allocation is properly performed according to the priority of the action zone and the distance between the action center and the vehicle.

- In relation to the duration of the exploration and exploitation phases, the analyses revealed that the proposed system showed good performance when the balance between the duration of the phases is between 50%/50% and 67%/37% of the maximum travel distance.

- Comparisons were made between a centralized learning-based system and the proposed FL-based system, and the results of model estimation and contamination peak detection for both systems turned out to be quite similar. However, FL allows for reduced data traffic between local

nodes and the main server [50]. In addition, in isolated areas, there is a possibility of having connection problems with the main server. On the other hand, by applying the FL technique, the GP adjustment will be performed by the local nodes. Moreover, by applying the FL technique in the second phase of informative path planning, each action zone has a different GP, which makes it possible to obtain a final water quality model even if the GP of one of the action zones does not converge [46].

- The lawnmower algorithm, due to the limitation of the maximum distance the ASVs can cover, failed to scan the entire lake surface. As a result, it was unable to detect pollution peaks or generate accurate models of the action zones and the water resource as a whole.

- The BO for multiple vehicles [22] employs an exploration approach that allows it to cover a significant portion of the surface area of the water resource. Nevertheless, its ability to detect contamination peaks may be less effective, as this task requires a focus on exploitation rather than exploration. Therefore, its performance in detecting contamination peaks may be relatively less efficient compared to other approaches.

- The Classic PSO [33] faces difficulties in detecting all pollution peaks due to its tendency to be trapped in local optima. This leads to the generation of unreliable estimated water quality models in the water resources monitoring process, since the monitoring task is a multi-modal problem.

- The Enhanced GP-based PSO, focusing on the exploration phase [24], succeeded in generating a satisfactory estimated model of the entire lake. However, it was not able to detect pollution peaks in the water resources, which limited its effectiveness in the monitoring task.

- The Enhanced GP-based PSO centered on the exploitation [25] succeeded in detecting the maximum contamination peak. However, due to the existence of several local and global peaks, the algorithm could not identify all peaks. Furthermore, by focusing on exploitation, it did not generate accurate water quality model estimates for either the polluted areas or the lake as a whole.

- The Epsilon greedy method showed robust performance in all three cases analyzed, thanks to its ability to switch approaches during the

monitoring task. This strategy change allowed the algorithm to effectively detect contamination peaks and generate high quality estimated models.

- The AquaFeL-PSO, the proposed informative path planner, outperformed all other planners compared. The water quality model for the contaminated areas obtained by the AquaFeL-PSO is 3% better than that of the epsilon-greedy method, which obtained the second best MSE. In addition, the water quality model of the entire water resource generated by the AquaFeL-PSO is at least 300% better than the second best MSE, also from the epsilon-greedy method. Regarding the detection of pollution peaks, the results obtained with the proposed informative path planner show an improvement of about 4000%. These improvements are due to the algorithm employing two controlled phases and dividing the map into specific zones for vehicles to exploit, thus dividing the fleet into sub-populations. The application of ANOVA test supports these improvements in peak detection and in the generation of the water quality model at the level of the entire water resource, demonstrating a significant difference between the means of the compared path planners. The model evaluation of the water quality parameters of the action zones indicates that there is no significant difference between the means of the compared path planners. Nonetheless, modeling the water quality parameters of the action zones is not as crucial as modeling the water quality parameters of the entire water resource and detecting pollution peaks. The latter two tasks are of greater importance in the overall approach to water resources monitoring.

- The proposed informative path planning offers two distinct mission approaches: exploration and exploitation, which facilitate the creation of a robust water quality model of the entire water resource. This approach allows not only to identify pollution peaks, but also to characterize in detail the water quality parameters in the affected areas. In addition, the use of federated learning principles provides each sub-fleet of ASVs with a unique Gaussian process. This ensures that a complete model of the water resource can be obtained even in cases of sub-fleet disconnection or non-convergence of a Gaussian process [46].

8. Conclusions

An informative path planning for water resource monitoring for ASVs was developed and simulated in this paper. The designed informative path planning is based on a multi-modal PSO and federated learning technique and uses the Gaussian process as a surrogate model. The objectives of the proposed informative path planning were to generate accurate estimated models of the contamination zones and the whole surface of the water resource, as well as the detection of contamination peaks. The AquaFeL-PSO algorithm has two phases, the exploration phase and the exploitation phase. In the exploration phase, the ASVs are dedicated to cover the surface of the water resource to obtain measurements from the water body and generate a first estimated water quality model. In the exploitation phase, using this first model generated, the surface of the water body is divided into action zones according to the length of the water resource and the number of vehicles in the fleet. Then, the ASVs are assigned to the action zones to carry out the exploitation of these areas. For the estimation of the water quality model of the action zones, the FL technique is used, which allows alleviating the data traffic between the nodes and the central server. Each action zone has its own node, and in each node the estimated model of that area is updated. Finally, when the monitoring task is completed, the models of the action zones are joined with the model obtained in the exploration phase to obtain the final water quality model of the water resource. It was demonstrated that with the AquaFeL-PSO it is possible to solve the multi-modal problem of water resource monitoring. The proposed informative path planning was able to detect pollution peaks and obtain accurate estimated water quality models of the action zones and the entire surface of the water body. As future work, the informative path planning developed will be improved to be able to determine the speed and direction of movement of the contamination zones in dynamic environments. Furthermore, a multi-objective PSO will be employed to obtain multiple water quality parameter models simultaneously. Therefore, the federated learning approach will be extended to the estimation of multiple models. Another future work is the implementation of the proposed informative path planning in real-world scenarios.

Appendix A. Appendix

This section shows the results obtained with two, six, and eight vehicles.

Appendix A.1. Proposed approach evaluation

Appendix A.1.1. Exploration vs Exploitation duration

This subsection details the results obtained for two (Table A.8), six (Table A.9) and eight vehicles (Table A.10) with respect to the duration of the exploration phase and the exploitation phase. Table A.8 shows the results obtained with two ASVs, when the maximum distance that ASVs can travel is 20km, the best combination of exploration and exploitation is 10km and 10km. This same result is obtained for six (Table A.9) and eight ASVs (Table A.10). Considering the maximum distance equal to 30km, the best result with two vehicles (Table A.8) was obtained in the Exploration 25km and Exploitation 5km. However, by a small margin, the second best was Exploration 15km and Exploitation 15km. For eight ASVs ((Table A.10)), similar results were obtained with Exploration 10km and Exploitation 20km, Exploration 15km and Exploitation 15km, and Exploration 20km and Exploitation 10km. It can be said that, with the balance between exploration and exploitation set at 50%/50%, a good performance of the algorithm is obtained. The best result with six ASVs (Table A.9) was obtained when the ASVs explored 20km and exploited 10km. However, the difference between the results obtained in the case Exploration 15km and Exploitation 15km case is very low. Therefore, it can be concluded that the best balance between exploration and exploitation is 50%/50% of the maximum distance, with cases where the distance of the exploration phase can be increased to 67% of the maximum travel distance. From the results obtained in Table A.10, it can be concluded that, having more vehicles, the difference is minimal whether the ASVs travel 20km or 30km. Therefore, the ideal distance for eight ASVs is 20km, since there is no significant difference in the results.

Table A.8: Comparison between the MSE of the distances traveled in the exploration phase and the exploitation phase for two vehicles

Vs	MSE 5km	MSE 10km	MSE 15km	MSE 20km	MSE 25km	MSE 30km
Exploration 5km	0.06180 ±	0.04020 ±	0.03476 ±	0.03425 ±	0.03403 ±	0.03395 ±
Exploitation 25km	0.05052	0.03669	0.03538	0.03635	0.03646	0.03656
Exploration 10km	0.06180 ±	0.02646 ±	0.01610 ±	**0.00622** ±	0.00574 ±	0.00562 ±
Exploitation 20km	0.05052	0.03128	0.02942	**0.02236**	0.01538	0.01123
Exploration 15km	0.06180 ±	0.02646 ±	0.01762 ±	0.01492 ±	0.00679 ±	**0.00375** ±
Exploitation 15km	0.05052	0.03128	0.02716	0.02734	0.01484	**0.01047**
Exploration 20km	0.06180 ±	0.02646 ±	0.01762 ±	0.01634 ±	0.01231 ±	0.00611 ±
Exploitation 10km	0.05052	0.03128	0.02716	0.02800	0.02511	0.01835
Exploration 25km	0.06180 ±	0.02646 ±	0.01762 ±	0.01634 ±	0.01253 ±	**0.00338** ±
Exploitation 5km	0.05052	0.03128	0.02716	0.02800	0.02214	**0.00857**
Exploration 30km	0.06180 ±	0.02646 ±	0.01762 ±	0.01634 ±	0.01253 ±	0.01077 ±
	0.05052	0.03128	0.02716	0.02800	0.02214	0.01879

Table A.9: Comparison between the MSE of the distances traveled in the exploration phase and the exploitation phase for six vehicles

Phase distance	MSE 5km	MSE 10km	MSE 15km	MSE 20km	MSE 25km	MSE 30km
Exploration 25km	0.00704 ±	0.00142 ±	0.00095 ±	0.00094 ±	0.00093 ±	0.00093 ±
Exploitation 15km	0.00701	0.00329	0.00198	0.00197	0.00198	0.00198
Exploration 10km	0.00704 ±	0.00276 ±	0.00065 ±	**0.00042** ±	0.00040 ±	0.00040 ±
Exploitation 20km	0.00701	0.00628	0.00194	**0.00097**	0.00092	0.00094
Exploration 15km	0.00704 ±	0.00276 ±	0.00201 ±	0.00060 ±	0.00050 ±	**0.00039** ±
Exploitation 15km	0.00701	0.00628	0.00538	0.00162	0.00168	**0.00128**
Exploration 20km	0.00704 ±	0.00276 ±	0.00201 ±	0.00136 ±	0.00043 ±	**0.00033** ±
Exploitation 10km	0.00701	0.00628	0.00538	0.00328	0.00103	**0.00085**
Exploration 25km	0.00704 ±	0.00276 ±	0.00201 ±	0.00136 ±	0.00113 ±	0.00052 ±
Exploitation 5km	0.00701	0.00628	0.00538	0.00328	0.00302	0.00149
Exploration 30km	0.00704 ±	0.00276 ±	0.00201 ±	0.00136 ±	0.00113 ±	0.00092 ±
	0.00701	0.00628	0.00538	0.00328	0.00302	0.00299

Table A.10: Comparison between the MSE of the distances traveled in the exploration phase and the exploitation phase for eight vehicles

Phase distance	MSE 5km	MSE 10km	MSE 15km	MSE 20km	MSE 25km	MSE 30km
Exploration 5km	0.00137 ±	0.00041 ±	0.00029 ±	0.00028 ±	0.00028 ±	0.00028 ±
Exploitation 25km	0.00196	0.00090	0.00056	0.00054	0.00054	0.00054
Exploration 10km	0.00137 ±	0.00023 ±	0.00006 ±	**0.00003** ±	0.00002 ±	**0.00002** ±
Exploitation 20km	0.00196	0.00044	0.00013	**0.00003**	0.00003	**0.00003**
Exploration 15km	0.00137 ±	0.00023 ±	0.00011 ±	**0.00003** ±	0.00002 ±	**0.00002** ±
Exploitation 15km	0.00196	0.00044	0.00035	**0.00004**	0.00003	**0.00003**
Exploration 20km	0.00137 ±	0.00023 ±	0.00011 ±	0.00006 ±	0.00005 ±	**0.00002** ±
Exploitation 10km	0.00196	0.00044	0.00035	0.00018	0.00019	**0.00004**
Exploration 25km	0.00137 ±	0.00023 ±	0.00011 ±	0.00006 ±	0.00005 ±	0.00006 ±
Exploitation 5km	0.00196	0.00044	0.00035	0.00018	0.00018	0.00028
Exploration 30km	0.00137 ±	0.00023 ±	0.00011 ±	0.00006 ±	0.00005 ±	0.00005 ±
	0.00196	0.00044	0.00035	0.00018	0.00018	0.00019

Appendix A.2. Performance comparison

The Tables A.11 and A.12 show the results obtained from the comparison of the path planners. Having a fleet with two vehicles, in the three case studies, the path planner that obtained the best performance was the proposed path planner. Unlike the results obtained with four vehicles, the difference in errors is not so large. However, the MSE of the estimated model of the whole lake and the error in the pollution peaks are up to 4 times lower than the second best MSE and error. With respect to the results obtained with six ASVs, in the modeling of the action zones, with a very small difference, the proposed path planner obtained the second best performance, behind the epsilon greedy method. However, in the other two case studies, the AquaFeL-PSO algorithm performed the best. In the detection of pollution peaks, the second best result is almost 20 times higher than the error obtained with the AquaFeL-PSO algorithm, and in the generation of the estimated model of the whole lake, the second best MSE is about 200% higher than the MSE of the proposed informative path planning.

Table A.11: Comparison of the MSE and the error of the path planners for two vehicles

Path Planner	MSE (Action Zones)	Error (Peaks)	MSE (Model of the Lake)
Lawn mower	0.06407 ± 0.11914	0.56516 ± 0.57607	0.04625 ± 0.03788
Classic PSO	0.05912 ± 0.11250	0.33411 ± 0.75806	0.04272 ± 0.05509
Enhanced GP-based PSO (Exploration)	0.03577 ± 0.06286	0.33622 ± 0.76587	0.01631 ± 0.02798
Enhanced GP-based PSO (Exploitation)	0.06164 ± 0.11393	0.36485 ± 0.80912	0.04378 ± 0.05145
Epsilon Greedy Method	0.04524 ± 0.08610	0.39966 ± 0.85490	0.03297 ± 0.04059
AquaFeL-PSO	**0.02361 ± 0.05634**	**0.07770 ± 0.44700**	**0.00526 ± 0.011230**

Table A.12: Comparison of the MSE and the error of the path planners for six vehicles

Path Planner	MSE (Action Zones)	Error (Peaks)	MSE (Model of the Lake)
Lawn mower	0.21101 ± 1.61966	0.27808 ± 1.20208	0.05738 ± 0.05048
Classic PSO	0.03357 ± 0.07676	0.06726 ± 0.25293	0.00450 ± 0.00609
Enhanced GP-based PSO (Exploration)	0.03472 ± 0.07295	0.04969 ± 0.19958	0.00131 ± 0.00313
Enhanced GP-based PSO (Exploitation)	0.03667 ± 0.08129	0.06685 ± 0.25677	0.00501 ± 0.00770
Epsilon Greedy Method	**0.03122 ± 0.06354**	0.05911 ± 0.25621	0.00200 ± 0.00385
AquaFeL-PSO	**0.03156 ± 0.06709**	**0.00255 ± 0.01590**	**0.00042 ± 0.00097**

References

[1] U. Desa, et al., Transforming our world: The 2030 agenda for sustainable development, United Nations (2016).

[2] Dirección General del Centro Multidisciplinario de Investigaciones Tecnológicas (CEMIT), Servicios de monitoreo de calidad de agua por campañas de muestreo en el lago ypacaraí. 2016 -2018, Tech. rep., Universidad Nacional de Asunción (UNA) (2018).

[3] Dirección General del Centro Multidisciplinario de Investigaciones Tecnológicas (CEMIT), Monitoreo de calidad de agua por campañas de muestreo en el lago ypacaraí 2019 - 2021, Tech. rep., Universidad Nacional de Asunción (UNA) (2021).

[4] G. A. López Moreira, L. Hinegk, A. Salvadore, G. Zolezzi, F. Hölker, R. A. Monte Domecq S, M. Bocci, S. Carrer, L. De Nat, J. Escribá,

et al., Eutrophication, research and management history of the shallow ypacaraí lake (paraguay), Sustainability 10 (7) (2018) 2426.

[5] M. Arzamendia, D. G. Reina, S. Toral, D. Gregor, E. Asimakopoulou, N. Bessis, Intelligent online learning strategy for an autonomous surface vehicle in lake environments using evolutionary computation, IEEE Intelligent Transportation Systems Magazine 11 (4) (2019) 110–125.

[6] S. Y. Luis, D. G. Reina, S. L. T. Marín, A multiagent deep reinforcement learning approach for path planning in autonomous surface vehicles: The ypacarac-lake patrolling case., IEEE Access (2021).

[7] C. Lin, G. Han, T. Zhang, S. B. H. Shah, Y. Peng, Smart underwater pollution detection based on graph-based multi-agent reinforcement learning towards auv-based network its, IEEE Transactions on Intelligent Transportation Systems (2022).

[8] F. Peralta, D. G. Reina, S. Toral, M. Arzamendia, D. Gregor, A bayesian optimization approach for water resources monitoring through an autonomous surface vehicle: The ypacarai lake case study, IEEE Access 9 (2021) 9163–9179. doi:10.1109/ACCESS.2021.3050934.

[9] F. Panetsos, P. Rousseas, G. Karras, C. Bechlioulis, K. J. Kyriakopoulos, A vision-based motion control framework for water quality monitoring using an unmanned aerial vehicle, Sustainability 14 (11) (2022) 6502.

[10] J. Sánchez-García, D. G. Reina, S. Toral, A distributed pso-based exploration algorithm for a uav network assisting a disaster scenario, Future Generation Computer Systems 90 (2019) 129–148.

[11] B. Song, Z. Wang, L. Zou, On global smooth path planning for mobile robots using a novel multimodal delayed pso algorithm, Cognitive Computation 9 (1) (2017) 5–17.

[12] F. Marini, B. Walczak, Particle swarm optimization (pso). a tutorial, Chemometrics and Intelligent Laboratory Systems 149 (2015) 153–165.

[13] M. J. Ten Kathen, I. J. Flores, D. G. Reina, An informative path planner for a swarm of asvs based on an enhanced pso with gaussian surrogate model components intended for water monitoring applications, Electronics 10 (13) (2021) 1605.

[14] F. Peralta, D. G. Reina, S. Toral, M. Arzamendia, D. Gregor, A bayesian optimization approach for multi-function estimation for environmental monitoring using an autonomous surface vehicle: Ypacarai lake case study, Electronics 10 (8) (2021) 963.

[15] S. Y. Luis, D. G. Reina, S. L. T. Marín, A deep reinforcement learning approach for the patrolling problem of water resources through autonomous surface vehicles: The ypacarai lake case, IEEE Access 8 (2020) 204076–204093.

[16] J. H. Holland, Genetic algorithms, Scientific american 267 (1) (1992) 66–73.

[17] O. Kramer, O. Kramer, Genetic algorithms, Springer, 2017.

[18] S. Sivanandam, S. Deepa, S. Sivanandam, S. Deepa, Genetic algorithms, Springer, 2008.

[19] M. Arzamendia, D. Gregor, D. G. Reina, S. L. Toral, An evolutionary approach to constrained path planning of an autonomous surface vehicle for maximizing the covered area of ypacarai lake, Soft Computing 23 (5) (2019) 1723–1734.

[20] M. Arzamendia, I. Espartza, D. G. Reina, S. Toral, D. Gregor, Comparison of eulerian and hamiltonian circuits for evolutionary-based path planning of an autonomous surface vehicle for monitoring ypacarai lake, Journal of Ambient Intelligence and Humanized Computing 10 (4) (2019) 1495–1507.

[21] S. Yanes Luis, D. Gutiérrez-Reina, S. Toral Marín, A dimensional comparison between evolutionary algorithm and deep reinforcement learning methodologies for autonomous surface vehicles with water quality sensors, Sensors 21 (8) (2021) 2862.

[22] F. Peralta, D. G. Reina, S. Toral, Water quality online modeling using multi-objective and multi-agent bayesian optimization with region partitioning, Mechatronics 91 (2023) 102953.

[23] F. Gul, W. Rahiman, S. Alhady, A. Ali, I. Mir, A. Jalil, Meta-heuristic approach for solving multi-objective path planning for autonomous guided robot using pso–gwo optimization algorithm with evolutionary

programming, Journal of Ambient Intelligence and Humanized Computing 12 (7) (2021) 7873–7890.

[24] M. J. Ten Kathen, I. J. Flores, D. G. Reina, A comparison of pso-based informative path planners for autonomous surface vehicles for water resource monitoring, in: 2022 7th International Conference on Machine Learning Technologies (ICMLT), 2022, pp. 271–276.

[25] M. J. Ten Kathen, D. G. Reina, I. J. Flores, A comparison of pso-based informative path planners for detecting pollution peaks of the ypacarai lake with autonomous surface vehicles, in: International Conference on Optimization and Learning OLA'2022, 2022.

[26] R. A. Khan, S. Yang, S. Khan, S. Fahad, et al., A multimodal improved particle swarm optimization for high dimensional problems in electromagnetic devices, Energies 14 (24) (2021) 8575.

[27] H. Wang, W. Wang, Z. Wu, Particle swarm optimization with adaptive mutation for multimodal optimization, Applied Mathematics and Computation 221 (2013) 296–305.

[28] X. T. Zhang, B. Xu, W. Zhang, J. Zhang, X. F. Ji, Dynamic neighborhood-based particle swarm optimization for multimodal problems, Mathematical Problems in Engineering 2020 (2020).

[29] X. Zhang, H. Liu, L. Tu, A modified particle swarm optimization for multimodal multi-objective optimization, Engineering Applications of Artificial Intelligence 95 (2020) 103905.

[30] W. D. Chang, A modified particle swarm optimization with multiple subpopulations for multimodal function optimization problems, Applied Soft Computing 33 (2015) 170–182.

[31] W.-D. Chang, Multimodal function optimizations with multiple maximums and multiple minimums using an improved pso algorithm, Applied Soft Computing 60 (2017) 60–72.

[32] W. Zhang, G. Li, W. Zhang, J. Liang, G. G. Yen, A cluster based pso with leader updating mechanism and ring-topology for multimodal multi-objective optimization, Swarm and Evolutionary Computation 50 (2019) 100569.

[33] J. Kennedy, R. Eberhart, Particle swarm optimization, in: Proceedings of ICNN'95-international conference on neural networks, Vol. 4, IEEE, 1995, pp. 1942–1948.

[34] Y. Shi, R. Eberhart, A modified particle swarm optimizer, in: 1998 IEEE international conference on evolutionary computation proceedings. IEEE world congress on computational intelligence (Cat. No. 98TH8360), IEEE, 1998, pp. 69–73.

[35] E. Schulz, M. Speekenbrink, A. Krause, A tutorial on gaussian process regression: Modelling, exploring, and exploiting functions, Journal of Mathematical Psychology 85 (2018) 1–16.

[36] C. E. Rasmussen, Gaussian processes in machine learning, in: Advanced Lectures on Machine Learning: ML Summer Schools 2003, Canberra, Australia, February 2-14, 2003, Tübingen, Germany, August 4-16, 2003, Revised Lectures, Springer, 2004, pp. 63–71.

[37] M. Wunder, M. L. Littman, M. Babes, Classes of multiagent q-learning dynamics with epsilon-greedy exploration, in: Proceedings of the 27th International Conference on Machine Learning (ICML-10), 2010, pp. 1167–1174.

[38] H. B. McMahan, E. Moore, D. Ramage, B. A. y Arcas, Federated learning of deep networks using model averaging, arXiv preprint arXiv:1602.05629 2 (2016).

[39] B. McMahan, E. Moore, D. Ramage, S. Hampson, B. A. y Arcas, Communication-efficient learning of deep networks from decentralized data, in: Artificial intelligence and statistics, PMLR, 2017, pp. 1273–1282.

[40] J. Konečnỳ, H. B. McMahan, F. X. Yu, P. Richtárik, A. T. Suresh, D. Bacon, Federated learning: Strategies for improving communication efficiency, arXiv preprint arXiv:1610.05492 (2016).

[41] J. Konečnỳ, H. B. McMahan, D. Ramage, P. Richtárik, Federated optimization: Distributed machine learning for on-device intelligence, arXiv preprint arXiv:1610.02527 (2016).

[42] M. Jara Ten Kathen, P. Johnson, I. Jurado Flores, D. Gutiérrez Reina, Monitoring peak pollution points of water resources with autonomous surface vehicles using a pso-based informative path planner, Mobile Robot: Motion Control and Path Planning (2023) –.

[43] Q. Yang, Y. Liu, Y. Cheng, Y. Kang, T. Chen, H. Yu, Federated learning, Synthesis Lectures on Artificial Intelligence and Machine Learning 13 (3) (2019) 1–207.

[44] M. Chen, H. V. Poor, W. Saad, S. Cui, Wireless communications for collaborative federated learning, IEEE Communications Magazine 58 (12) (2020) 48–54.

[45] D. Ye, R. Yu, M. Pan, Z. Han, Federated learning in vehicular edge computing: A selective model aggregation approach, IEEE Access 8 (2020) 23920–23935.

[46] M. J. T. Kathen, F. Peralta, P. Johnson, I. Jurado Flores, D. Gutiérrez Reina, Performance evaluation of aquafel-pso informative path planner under different contamination profiles, in: Data Analytics and Computational Intelligence: Novel Models, Algorithms and Applications, Springer, 2023, pp. 405–431.

[47] V. Bewick, L. Cheek, J. Ball, Statistics review 9: one-way analysis of variance, Critical care 8 (2004) 1–7.

[48] A. Grafen, R. Hails, Modern statistics for the life sciences, Oxford University Press, 2002.

[49] H.-Y. Kim, Analysis of variance (anova) comparing means of more than two groups, Restorative dentistry & endodontics 39 (1) (2014) 74–77.

[50] J. C. Jiang, B. Kantarci, S. Oktug, T. Soyata, Federated learning in smart city sensing: Challenges and opportunities, Sensors 20 (21) (2020) 6230.

[51] A. Sakai, D. Ingram, J. Dinius, K. Chawla, A. Raffin, A. Paques, Pythonrobotics: a python code collection of robotics algorithms, arXiv preprint arXiv:1808.10703 (2018).

[52] J. Xin, S. Li, J. Sheng, Y. Zhang, Y. Cui, Application of improved particle swarm optimization for navigation of unmanned surface vehicles, Sensors 19 (14) (2019) 3096.

[53] Y. Cui, J. Zhong, F. Yang, S. Li, P. Li, Multi-subdomain grouping-based particle swarm optimization for the traveling salesman problem, IEEE Access 8 (2020) 227497–227510.